

## Water and Vapor Transport in Algal-Fungal Lichen

### Modeling constrained by Laboratory Experiments, an application for *Flavoparmelia caperata*

Potkay, Aaron; ten Veldhuis, Marie-Claire; Fan, Ying; Mattos, Caio R.C.; Ananyev, Gennady; Dismukes, Charles

**DOI**

[10.1111/pce.13690](https://doi.org/10.1111/pce.13690)

**Publication date**

2019

**Document Version**

Final published version

**Published in**

Plant, Cell & Environment

**Citation (APA)**

Potkay, A., ten Veldhuis, M.-C., Fan, Y., Mattos, C. R. C., Ananyev, G., & Dismukes, C. (2019). Water and Vapor Transport in Algal-Fungal Lichen: Modeling constrained by Laboratory Experiments, an application for *Flavoparmelia caperata*. *Plant, Cell & Environment*, 43 (2020)(4), 945-964.  
<https://doi.org/10.1111/pce.13690>

**Important note**

To cite this publication, please use the final published version (if applicable).  
Please check the document version above.

**Copyright**

Other than for strictly personal use, it is not permitted to download, forward or distribute the text or part of it, without the consent of the author(s) and/or copyright holder(s), unless the work is under an open content license such as Creative Commons.

**Takedown policy**

Please contact us and provide details if you believe this document breaches copyrights.  
We will remove access to the work immediately and investigate your claim.



***Green Open Access added to TU Delft Institutional Repository***

***'You share, we take care!' - Taverne project***

**<https://www.openaccess.nl/en/you-share-we-take-care>**

Otherwise as indicated in the copyright section: the publisher is the copyright holder of this work and the author uses the Dutch legislation to make this work public.

# Water and vapor transport in algal-fungal lichen: Modeling constrained by laboratory experiments, an application for *Flavoparmelia caperata*

Aaron Potkay<sup>1</sup>  | Marie-Claire ten Veldhuis<sup>2,3</sup>  | Ying Fan<sup>1</sup> |  
Caio R. C. Mattos<sup>1</sup> | Gennady Ananyev<sup>3,4</sup> | G. Charles Dismukes<sup>3,4</sup>

<sup>1</sup>Department of Earth and Planetary Sciences, Rutgers University

<sup>2</sup>Water Management Department, Delft University of Technology

<sup>3</sup>Waksman Institute of Microbiology, Rutgers University

<sup>4</sup>Department of Chemistry and Chemical Biology, Rutgers University

## Correspondence

Aaron Potkay, Department of Earth and Planetary Sciences, Rutgers University.  
Email: ajp360@eps.rutgers.edu

## Funding information

Basic Energy Sciences; Department of Energy

## ABSTRACT

Algal-fungal symbionts share water, nutrients, and gases via an architecture unique to lichens. Because lichen activity is controlled by moisture dynamics, understanding water transport is prerequisite to understand their fundamental biology. We propose a model of water distributions within foliose lichens governed by laws of fluid motion. Our model differentiates between water stored in symbionts, on extracellular surfaces, and in distinct morphological layers. We parameterize our model with hydraulic properties inverted from laboratory measurements of *Flavoparmelia caperata* and validate for wetting and drying. We ask: (1) Where is the bottleneck to water transport? (2) How do hydration and dehydration dynamics differ? and (3) What causes these differences? Resistance to vapor flow is concentrated at thallus surfaces and acts as the bottleneck for equilibrium, while internal resistances are small. The model captures hysteresis in hydration and desiccation, which are shown to be controlled by nonlinearities in hydraulic capacitance. Muting existing nonlinearities slowed drying and accelerated wetting, while exaggerating nonlinearities accelerated drying and slowed wetting. The hydraulic nonlinearity of *F. caperata* is considerable, which may reflect its preference for humid and stable environments. The model establishes the physical foundation for future investigations of transport of water, gas, and sugar between symbionts.

## KEYWORDS

*Flavoparmelia caperata*, hydraulic limitations, lichen, modeling, Symbiosis, water relations

## 1 | INTRODUCTION

Lichens are pioneer symbiotic organisms of primary succession that can survive in all terrestrial environments, including those with extreme climates such as the Arctic, Antarctic, high alpine, and desert (Ahmadjian, 1993; Longton, 1988), and they dominate ~10% of the Earth's land surface (Honegger, 2006), particularly in marginal environments. Lichens contribute to the local and global carbon budget (Ahmadjian, 1995) and may have played a critical role during the development of the early terrestrial landscape before higher plants colonized the land (Selosse, 2002; Selosse, Strullu-Derrien, Martin,

Kamoun, & Kenrick, 2015). Periods of lichens' photosynthesis and growth are limited by the duration and frequency of their hydrated, active periods (Dahlman & Palmqvist, 2003; Palmqvist & Sundberg, 2000), and the magnitude of their photosynthetic assimilation is suppressed at low thallus water contents (Lange, Green, & Heber, 2001). Since lichens lack the ability to prevent desiccation, they are termed poikilohydric, and their water uptake and loss lack metabolic control (Blum, 1973). Instead, they passively equilibrate with their surroundings (Rundell, 1982), particularly with the water potential of the air (Rundel, 1998; Jonsson, Moen, & Palmqvist, 2008). Periods of hydration are prolonged by surface resistance to vapor flow

(Monteith, 1965) and by internal resistance within the thallus (Kershaw, 1985) associated with thalli morphology and anatomy (Honegger, 2006). Shrinkage and swelling of the thallus occur during drying and wetting cycles (Honegger, 2006). These volume changes are known to generate additional resistance to water flow in other porous media and influence the rate at which they wet and dry (Philip, 1969; Potkay, 2017; Smiles & Rosenthal, 1968) by altering water storage, capacitance, conductance, and the lengths of flow paths.

About 25% of all lichen-forming fungi have developed morphologically and anatomically complex differentiation, forming leaf- or shrub-like symbiotic phenotypes (Honegger, 1998). These so-called macrolichens form complex structures with internal stratification generally consisting of a dense upper cortex, a thin layer just below the upper cortex where photobiont cells are concentrated and a thicker medulla layer of loosely woven fungal hyphae (Honegger, 1991). The main structural components of the mycobiont are: (1) pseudoparenchyma that provides mechanical stability to the thallus and is often found in the form of peripheral cortical layers and/or central strands covered with hydrophilic material at the wall surface, and (2) plectenchyma, usually consisting of loosely interwoven aerial hyphae (filaments) with mainly hydrophobic cell wall surfaces that are postulated to help maintain gas-filled spaces in the thallus interior for gas transport. In many lichen-forming ascomycetes, the cell wall of the fungal hyphae is covered by a thick wall comprised of polyglucans that are hydrophilic, and absorb and retain high amounts of water. These polyglucans are believed to play an important role in water relations in the lichen thallus (Honegger, 2012; Honegger & Haisch, 2001).

Understanding and predicting photosynthesis (light driven  $\text{CO}_2$  fixation rate and flux) and growth of lichen requires accurate description of the duration, magnitude, and spatial distribution of thallus hydration. Existing models of lichen hydration and productivity are primarily empirical (Coxson, 1991; Dahlman & Palmqvist, 2003; Lange, Geiger, & Schulze, 1977; Palmqvist & Sundberg, 2000; Paterson, Paterson, & Kenworthy, 1983; Sundberg, Näsholm, & Palmqvist, 2001), offer little insight to the underlying mechanisms, and have limited predictive power under changing environmental conditions. Photosynthesis is often regressed as function of bulk thallus water content (Lange et al., 1977; Paterson et al., 1983), despite that photosynthetic potential should depend on the hydration status of the photobiont and not the entire thallus. Photosynthesis in vascular plants is often modeled as a Michaelis–Menten function of the carbon dioxide concentration in the chloroplasts (Farquhar, von Caemmerer, & Berry, 1980; Tenhunen, Yocum, & Gates, 1976). A similar approach would provide deeper insights into the fundamental biology of lichen. Applying a photosynthesis model like Farquhar et al. (1980) to lichen would require first estimating the carbon dioxide concentration in the chloroplasts in the photobionts and consequently the thallus's resistance to the carbon dioxide transport, which depends on the saturation of "external" pathways (apoplast; Eriksson, Gauslaab, Palmqvista, Ekström, & Esseen, 2018), because of the inherently slower diffusion of gasses in water than in air (Green, Sancho, & Pintado, 2011; Lange et al., 1993, 2001). Estimating the photobiont's carbon dioxide concentration is further complicated by the possibility of gas recycling

between mycobiont and photobiont. Under this framework, the turning off of lichen photosynthesis under desiccation (Lange et al., 2001) could be explained by the reduction in maximum photosynthetic potential ( $V_{\text{cmax}}$  and  $J_{\text{max}}$  in Farquhar et al., 1980) under highly negative matric water potentials (Vico & Porporato, 2008) or under excess sugar concentrations (Hölttä, Lintunen, Chan, Mäkelä, & Nikinmaa, 2017) in the photobiont. We believe that this type of photosynthesis model in coordination with a model framework that distinguishes between photobiont and mycobiont as separate water reservoirs may also be able to describe the time-lag between the onset of bulk lichen saturation and the turning on of photosynthesis during wetting (Jonsson-Čabrajić, Lidén, Lundmark, Ottosson-Löfvenius, & Palmqvist, 2010; Lidén, Jonsson-Čabrajić, Ottosson-Löfvenius, Palmqvist, & Lundmark, 2010). Simulating dynamic lichen photosynthesis in response to fluctuating water availability will require differentiating the hydration status of mycobiont and photobiont to describe the transport of water and gasses through various pathways within the thallus and to describe the various phenomenon in lichen photosynthesis, namely (1) the suppression of photosynthesis at low water contents, (2) suppression of photosynthesis at supersaturated water contents where gas diffusion is limited, and (3) the time-lag for photosynthetic activity to peak after initial wetting.

In this study, we attempt to describe the fluxes of water within the interior of the lichen thallus in a manner mathematically similar to the mass transfer approaches that govern the dynamics of moisture in soil and other porous media (e.g., Richards equation; Richardson, 1922; Richards, 1931). Flow of water in variably saturated porous media is the product of the hydraulic conductivity and the gradient in water potential (Darcy's law). The conductivity is a material property of the porous media that reflects the size of pores and their distribution (e.g., Hagen–Poiseuille equation) and the degree to which they are filled with water (e.g., van Genuchten, 1980). As soil moisture equilibrates with its surroundings, the magnitudes of gradients gradually decline, and flow velocities adjust until a steady-state is achieved. However, knowing the flow rate is not enough by itself to describe the moisture dynamics of a porous media. The flow rate only describes how quickly the moisture levels change but says nothing about how water potentials change in time, which govern subsequent flow rates and therefore subsequent moisture levels. Assuming the environmental conditions is known, the only missing piece of information required to describe the system in full is either the media's water retention curve, the relationship between water content and potential, or the hydraulic capacitance, which is the slope of this curve and a measure of the media's ability to store water and the sensitivity of water storage to water fluxes.

In soils, water retention and hydraulic capacitance reflect the distribution of pore-sizes and the capillarity associated with the surface tension between pore-water and pore-wall (Jurin's law). However, the water retention and hydraulic capacitance of lichen tissue also likely reflect the elasticity of cell walls (e.g., Eqn 2 in Thompson and Holbrook, 2003), the packing of filaments and cells, and thallus thickness (Sveinbjörnsson, 1987). The water retention curves of soils and lichen do not differ significantly in shape (Voortman et al., 2014). However, the magnitude of their curves (and resulting capacitances) may differ by more than an order of

magnitude, because soils typically rarely exceed a water content of 120% (percent of dry weight; assuming porosity of 0.5 and mineral specific gravity of 2.7), while the water content of lichen thalli can exceed 1600% (e.g., Fig. 2 in Lange et al., 2001). High capacitance is a common strategy of vascular plants to avoid desiccation (McCulloh, Johnson, Meinzer, & Woodruff, 2014; Meinzer, Johnson, Lachenbruch, McCulloh, & Woodruff, 2009). Presumably, lichens employ high capacitance as a strategy to prolong wet, active periods when photosynthesis can occur (Dahlman & Palmqvist, 2003; Palmqvist & Sundberg, 2000). This hypothesis is supported by evidence that the productivity of lichens is enhanced by the formation of thick, dense thalli that act as water reservoirs (; Helle, Aspi, & Tarvainen, 1983; Kershaw & Rouse, 1971; Sveinbjörnsson, 1987; Gauslaa & Solhaug, 1998).

There exist few models that describe the temporal dynamics of lichen wetting and drying from environmental inputs (e.g., Jonsson et al., 2008; Lloyd, 2001; Paterson et al., 1983; Péch, 1989). These models describe vapor transport between the thallus and the surrounding air, and how quickly the bulk thallus water content equilibrates. They do not attempt to describe the distribution of water reservoirs within the thallus either spatially or within separate symbionts. In this study, we distinguish between the water-status of symbionts, since lichen-photosynthesis depends only on the status of the photobiont, distinct morphological layers (cortices, medulla, and photobiont), and liquid and vapor phases of water. Additionally, our model includes a reservoir for extracellular pore-water which may restrict gas transport and depress photosynthesis due to the inherently slower diffusion of gasses in water than in air (Green et al., 2011; Lange et al., 1993, 2001). Existing models have three general types of deficiencies which we seek to correct. First are those that neglect the fundamental physics of vapor flow, which should be a vapor pressure-driven flow problem (Dalton's law). For example, past models have instead assumed vapor flow rates linearly proportional to the difference between current and equilibrium water contents (Jonsson et al., 2008) and as empirical functions of time (Péch, 1989). Second are those that ignore water content's dependence on water potential. Instead, past models have simulated water content from regressions with the air's relative humidity (Péch, 1989), which ignores the influence of temperature and the disequilibrium in relative humidity between lichen and air, and vapor pressure deficit (Paterson et al., 1983), which would rather better explain how quickly the lichen wets or dries. The lack of physics leads to the third problem: heavy dependence on empirically fitted relations with numerous parameters that are hard-wired into the model (Jonsson et al., 2008; Paterson et al., 1983; Péch, 1989). For example, the asymmetry of wetting and drying has to be prescribed and forced with different sets of coefficients (Jonsson et al., 2008). Our model explains and predicts the hysteresis in wetting and drying dynamics through the underlying physics of fluid flow in deforming, porous media (Philip, 1969; Potkay, 2017; Smiles & Rosenthal, 1968), particularly the strong nonlinear dependence of hydraulic capacitance on water content (Coxson, 1991). We have designed the model such that we can extend the model to incorporate gas ( $\text{CO}_2$  and  $\text{O}_2$ ) and solute (sucrose) transport through internal and external pathways, respiration within metabolically active portions of the thallus (both mycobiont and

photobiont), and photosynthesis within the photobiont using a Farquhar-type model (Farquhar et al., 1980).

We estimate model parameters from laboratory measurements on *Flavoparmelia caperata* and validate our model by comparing simulations and observations of desiccation and hydration dynamics of the same species. We apply our model to ask the following questions: (1) Where is the bottleneck to water transport in the lichen thallus? (2) How do hydration and dehydration dynamics differ? and (3) What causes these differences? Concerning question (1), we hypothesize that vapor transport between the atmosphere and the lichen at its cortices is the dominant control on how quickly bulk thallus water content equilibrates with its surroundings. We were led to this first hypothesis by the general consensus that lichen develops dense cortices to restrict evaporation (Kershaw & Rouse, 1971; Helle et al., 1983; Gauslaa & Solhaug, 1998). Though not explicitly stated, previous models implicitly assume this first hypothesis (Jonsson et al., 2008; Paterson et al., 1983; Péch, 1989), which has not been previously tested in a framework that includes internal water transport. Concerning questions (2) and (3), we further hypothesize that the difference in the time-scales for wetting and drying is a product of the strong nonlinearities in the hydraulic capacitance of the lichen thallus. We frame this second hypothesis in terms of hydraulic capacitance for two reasons: to highlight its importance as a driver of hydration dynamics and as means of prolonging productivity under dry conditions, and because past models neglect its influence on vapor transport dynamics between thallus and atmosphere by ignoring the underlying physics.

## 2 | MATERIALS AND METHODS

Many physiological properties necessary for our model can be constrained by values reported in the literature; however, two key relationships are specific to our lichen samples. These relationships are (1) how evaporation and condensation rates relate to differences in water vapor partial pressure between the lichen surface and bounding air (vapor conductance) and (2) how much water the lichen thallus retains under declining water potential (water retention). We estimated these relationships through inversion of laboratory observations from a single desiccation experiment performed on initially saturated samples of *F. caperata* that equilibrated with the surrounding air's water potential. Though we constrained model parameters from a single experiment, we performed multiple of these desiccation experiments under a range of water potentials as well as a hydration experiment to validate the model for both wetting and drying regimes.

### 2.1 | Lichen desiccation experiments

We chose *F. caperata*, a symbiosis between an ascomycete fungus and the green algal photobiont *Trebouxia gelatinosa* (Ahmadjian, 1993), for laboratory observation and modeling. Lichen samples were collected in spring season from the bark of mature maple trees in Princeton, New Jersey, USA. Thallus samples were stored at room

temperature and 0.40–0.50 relative humidity. Disk-shaped samples of 7 mm diameter and approximately 100  $\mu\text{m}$  thickness were cut from the youngest part of the lichen leaf. For the real-time dehydration experiments, samples of 7 mm diameter were immersed in distilled water for 5 min or longer to reach full hydration, then pat-dried and placed on the gravimeter to immediately start the experiment. Weight loss dynamics were measured until stable weight conditions were reached. Five replicate experiments were conducted, with atmospheric potential values varying between  $-92$  and  $-148$  MPa. The relative humidity of each experiment was assumed to be equal to the ambient relative humidity, which did not change significantly. In the gravimeter, samples sat on a porous, foam block that likely would not prevent evaporation from the bottom side of the lichen.

## 2.2 | Lichen hydration experiment

One hydration experiment was performed to validate our model's simulation of wetting dynamics. A 7 mm diameter lichen sample was immersed in distilled water for 5 min to reach full hydration, then pat-dried and placed on the gravimeter to equilibrate with the air's water potential in the laboratory (0.21 RH and 26 °C) over 30 min. Once the thallus mass reached equilibrium, we placed a dish filled with water next to the gravimeter and a hygrometer above the chamber of the gravimeter. In the gravimeter, the lichen sample rested inside a small cavity exposed only at the top. This space was too small to fit the hygrometer inside. Instead, the hydrometer was placed immediately above the gravimeter's opening. We added wetted cloths to the water dish to increase its evaporative surface area. We immediately covered the gravimeter, hygrometer, and water dish inside a translucent, plastic chamber ( $\sim 0.3$  m by  $\sim 0.5$  m and  $\sim 0.3$  m deep) and sealed the edges to begin the experiment. Thallus mass was measured continuously for 2.5 h and the relative humidity and temperature with the chamber was measured periodically. We designed the hydration experiment such that the water dish would evaporate, slowly raising the relative humidity of the chamber once sealed, and that we could observe the resulting change in thallus mass as water potentials equilibrated.

## 2.3 | Estimation of lichen hydraulic properties

First, we estimated  $\beta$  [ $\text{m s}^{-1} \text{Pa}^{-1}$ ], a measure of aerodynamic resistance to vapor exchange between the lichen surface and the air. It is the constant in the linearized form of Dalton's law of evaporation (Penman, 1948), defined as the slope of relationship between bulk lichen evaporation rate,  $E$  [ $\text{m s}^{-1}$ ], and difference in partial vapor pressures between lichen and surrounding air,  $\Delta P_v$  [Pa] (see also abbreviations and definitions of all model variables in Table 1).

$$E = \beta \Delta P_v \quad (1)$$

$\beta$  depends on surface roughness and changes as a function of windspeed. Laboratory experiments were performed indoors, and we

assume the influence of wind to be either negligible or constant, and in either case,  $\beta$  may be approximated as a constant. We performed linear regression on the initial evaporation rates as a function of the initial vapor pressure difference from multiple desiccation experiments performed under various air relative humidities, and we assume this relationship holds true through the entire duration of desiccation as well as when dry lichen is wetted by humid air. We chose to regress only initial values of evaporation rates and vapor pressure differences, because the vapor pressure difference is known a priori only at the very beginning of each experiment when the thallus is fully saturated and when the total (sum of matric and osmotic potentials) water potential may be approximated as zero. Initial evaporation rates were calculated from the change in thallus mass during desiccation experiments averaged over the first 2–3 min when evaporation rates were near constant. We assume an osmolyte concentration of 0.890 M based on measurements by Kosugi et al. (2014) for other lichen species and calculated by the van't Hoff equation for osmotic potential. Though Kosugi et al.'s (2014) data are for a different lichen species, our results are relatively insensitive to the assumed osmolyte concentration, since (1) the corresponding potential is an order of magnitude less than range of air water potentials occurred in our laboratory experiments, and (2) the range of osmolyte concentrations of various lichen species with green algae photobionts reported in the literature is small (0.85–0.93 M; reviewed in Kosugi et al., 2014). The initial matric potential,  $\psi_m$  [m], of the lichen top and bottom surfaces was assumed equal to the negative of the osmotic potential, since the initial total water potential may be approximated as zero. Note that we express potentials as hydraulic head (i.e., units of length) rather than in traditional units of pressure. Head and pressure are related through the acceleration due to gravity and the density of water. The thallus temperature,  $T$  [K], was assumed equal to the measured air temperature. The saturated vapor pressure of both air and thallus were calculated by Tetens's (1930) equation. The relative humidity of the air was measured directly, and the relative humidity,  $RH$  [–], of the lichen surface was calculated by Philip and de Vries' (1957) equation

$$RH = \exp\left(\frac{\psi_m g M_w}{RT}\right) \quad (2)$$

where  $g$  is the acceleration due to gravity [ $\text{m s}^{-2}$ ],  $M_w$  is the molar mass of water [ $\text{kg mol}^{-1}$ ], and  $R$  is the universal gas constant [ $\text{J K}^{-1} \text{mol}^{-1}$ ]. Because we estimated  $\beta$  from bulk thallus mass changes during desiccation,  $\beta$  represents the sum conductance (in parallel) of water vapor through both top and bottom sides of the thallus and cannot distinguish between each side's contribution to conductance. We assume water vapor may escape or enter from both sides, and for simplicity we assume the conductances of each side are equal despite that the top and bottom conductances likely differ in actuality due to thallus physiology (Ten Veldhuis, Dismukes, & Ananyev, 2017).

Second, we estimated the relationship between water content (expressed here as water ratio,  $\theta$ , or the volume-ratio of stored water to nonfluid phases) and the fluid potential which drives flow. We

**TABLE 1** Mathematical terms and definitions, abbreviations, and units, used in estimation of lichens' hydraulic properties and presented in model details in Supporting Information. Values and literature sources are given when appropriate

Name	Symbol	Unit	Value	Source
Material coordinate	$m$	[m]		Smiles and Rosenthal (1968); Philip (1969)
Maximum, compacted thallus thickness	$M$	[m]		
Cartesian coordinate	$z$	[m]		
Thallus thickness	$Z$	[m]		
Cartesian thicknesses of morphological layers under complete saturation		[ $\mu\text{m}$ ]		
Upper cortex			30	Estimated from dimensions of lichen sample
Photobiont layer			20	Estimated from dimensions of lichen sample
Medulla			40	Estimated from dimensions of lichen sample
Lower cortex			30	Estimated from dimensions of lichen sample
Time	$t$	[s]		
Bulk two-sided evaporation rate	$E$	[ $\text{m s}^{-1}$ ]		Measured
Bulk two-sided conductance to water vapor	$\beta$	[ $\text{m s}^{-1} \text{Pa}^{-1}$ ]	$7.342 \times 10^{-11}$	Estimated from initial evaporation rates (see Methods)
Local evaporation rates at upper boundary	$E_{F,\text{top}}, E_{P,\text{top}}$	[ $\text{m s}^{-1}$ ]		Dalton's law of evaporation using estimated $\beta/2$ as conductance to vapor flow
Local evaporation rates at lower boundary	$E_{F,\text{bottom}}, E_{P,\text{bottom}}$	[ $\text{m s}^{-1}$ ]		Dalton's law of evaporation using estimated $\beta/2$ as conductance to vapor flow
Vapor pressure difference between bulk lichen and air	$\Delta P_v$	[Pa]		
Saturated vapor pressure	$P_{v,\text{sat}}$	[Pa]		Tetens (1930)
Vapor pressure of air and local thallus compartments	$P_{v,a}, P_{v,F}, P_{v,P}$	[Pa]		Calculated from $P_{v,\text{sat}}$ and appropriate $RH$
Relative humidity of air	$RH$	[-]		Measured
Local relative humidities	$RH_F, RH_P$	[-]		
Saturated vapor density	$\rho_{v,\text{sat}}$	[ $\text{kg m}^{-3}$ ]		Tetens (1930) and ideal gas law
Density of liquid water	$\rho_w$	[ $\text{kg m}^{-3}$ ]	1000	
Acceleration due to gravity	$g$	[ $\text{m s}^{-2}$ ]	9.81	
Molecular weight of water	$M_w$	[ $\text{kg mol}^{-1}$ ]	$1.8 \times 10^{-3}$	
Universal gas constant	$R$	[ $\text{J mol}^{-1} \text{K}^{-1}$ ]	8.314	
Air temperature (assumed for lichen)	$T$	[ $^{\circ}\text{C}$ ]		Measured
Bulk void-ratio	$e$	[-]		
Local void-ratios	$e_F, e_A, e_P$	[-]		
Maximum local void-ratios	$e_{F,\text{max}}, e_{A,\text{max}}, e_{P,\text{max}}$	[-]	2000, 2000, 2000	Interpreted from Lesmerises, Ouellet, and St-Laurent (2011); Fig. 1) assuming density of solids may be approximated as the density of cellulose
Minimum local void-ratios	$e_{F,\text{min}}, e_{A,\text{min}}, e_{P,\text{min}}$	[-]	0, 0, 2000	Approximated as zero for fungus and algae; approximated by maximum for pores assuming that the geometry of pores is rigid
Bulk water-ratio	$\vartheta$	[-]		
Local water-ratios	$\vartheta_F, \vartheta_A, \vartheta_P$	[-]		
Bulk effective saturation	$S_e$	[-]		
Local effective saturations	$S_{e,F}, S_{e,A}, S_{e,P}$	[-]		Asymptotic fitting equation (Eqn 3) with shaping parameters ( $a_1 = 5.18 \times 10^{-4} \text{m}^{-1}$ , $a_2 = 2.77 \times 10^{-3} \text{m}^{-1}$ , $b = -1.17 \times 10^3 \text{m}$ , $c = 0.862$ ) estimated by bulk response of thallus from single 0.34 $RH$ desiccation experiment (see Methods)

(Continues)

TABLE 1 (Continued)

Name	Symbol	Unit	Value	Source
Volume-weighting factors	$W_F, W_A, W_P$	[-]		Estimated from photos by Honegger (2006, 2012)
<i>Upper cortex</i>			0.9, 0, 0.1	
<i>Photobiont layer</i>			0.4, 0.4, 0.2	
<i>Medulla</i>			0.5, 0, 0.5	
<i>Lower cortex</i>			0.9, 0, 0.1	
Vertical (within compartment) water fluxes	$q_{w,F}, q_{w,P}$	$[m\ s^{-1}]$		Darcy's law and modified form of Dalton's law of evaporation
Local matric water potentials	$\psi_{m,F}, \psi_{m,A}, \psi_{m,P}$	[m]		
Local osmotic water potentials	$\psi_{o,F}, \psi_{o,A}, \psi_{o,P}$	[m]	-220	Based on a 0.890 M osmolyte concentration from Kosugi et al. (2014) at 25 °C
Local total water potentials	$\psi_{t,F}, \psi_{t,A}, \psi_{t,P}$	[m]		
Local hydraulic conductivities	$K_F, K_P$	$[m\ s^{-1}]$		$K_F$ modeled by Hagen–Poiseuille equation modified by Thompson and Holbrook (2003) to describe resistance associated with septal-pores; $K_P$ modeled by van Genuchten (1980) functions of effective saturation with fitting parameters from Voortman et al. (2014)
Maximum pore-space conductivity	$K_{P,max}$	$[m\ s^{-1}]$	$2.3 \times 10^{-8}$	Voortman et al. (2014)
van Genuchten's pore connectivity term	$l_{VG}$	[-]	-2.7	Voortman et al. (2014)
van Genuchten's <i>m</i>	$m_{VG}$	[-]	0.54	Voortman et al. (2014)
Kinematic viscosity of water	$\nu$	$[m^2\ s^{-1}]$	$1 \times 10^{-6}$	
Sampson factor	$\varphi$	[-]		Thompson and Holbrook (2003)
Septal-pore factor	$\chi$	[-]		Thompson and Holbrook (2003)
Fungal filament and alga radii	$r_F, r_A$	[m]		
Radius of septal-pores connecting fungal cells	$r_{F,sept}$	[m]	$1 \times 10^{-7}$	Estimated from photos by Sanders and Ríos (2017)
Distance between septal walls	$d_F$	[m]	$4 \times 10^{-6}$	Estimated from photos by Sanders and Ríos (2017)
Thickness of septal walls	$d_{F,sept}$	[m]	$3 \times 10^{-7}$	Estimated from photos by Sanders and Ríos (2017)
Isothermal vapor hydraulic conductivity of pores	$D_{v,P}$	$[m\ s^{-1}]$		Heitman et al. (2008)
Diffusivity of water vapor in air	$D_v$	$[m^2\ s^{-1}]$	$2.12 \times 10^{-5}$	
Tortuosity of air within extracellular pores	$\tau_{a,P}$	[-]		Lai, Tiedje, and Erickson (1976)
Horizontal (among compartment) water fluxes	$\Gamma_{w,1}, \Gamma_{w,2}, E_1$	$[m\ s^{-1}]$		Darcy's law and modified form of Dalton's law of evaporation
Dimensions of representative lichen volume	$\Delta x, \Delta y, \Delta z$	[m]		
Total surface area of fungal and algal cells	$\Sigma A_F, \Sigma A_A$	$[m^2]$		
Cross-sectional area of representative volume transverse to direction of lateral flow	$A_{yz}$	$[m^2]$		
Lateral length scales	$l_F, l_A, l_P$	[m]		
Maximum fungal filament and alga radii	$r_{F,max}, r_{A,max}$	[m]	$1 \times 10^{-6}, 4 \times 10^{-6}$	Estimated from photos by Honegger (2006, 2012)
Volumetric elastic modulus	$\varepsilon$	[Pa]		
Interface conductance	$k_1, k_2$	$[s^{-1}]$		$k_1$ modeled as conductance of cellular membrane of fungal filaments; $k_2$ modeled as conductance across mycobiont-photobiont interfaces, including hyphae and intragelatinous protrusions

(Continues)



**TABLE 1** (Continued)

Name	Symbol	Unit	Value	Source
Conductance of fungal filaments' cellular membrane	$k_{\text{cell},F}$	$[\text{s}^{-1}]$	$1 \times 10^{-9}$	Estimated as membrane conductance of sieve-tube walls and parenchyma of higher plants (Kim & Steudle, 2007; Lang, 1978; Tyree, 1970)
Radius of mycobiont-photobiont interface	$r_{F-A}$	[m]	$1 \times 10^{-7}$	Assumed equal to radius of septal-pores, $r_{F,\text{sept}}$

represent water content by water-ratio rather than the more common weight-ratio to simplify the mathematics, particularly for swelling media since the volume of nonfluid phases should be reasonably constant (see Supporting Information). The relationship between water content and potential describes the quantity of water the bulk lichen thallus retains under increasing water stress, and can be obtained by reinterpreting the previously mentioned desiccation experiments through the estimated relationship between evaporation rate and vapor pressure difference, namely our estimated  $\beta$ . This method involves simultaneously interpreting two variables from the data, namely the thalli's effective saturation,  $S_e$  [-], which is the water content scaled between residual and maximum water contents (0 to 1), and the matric potential of the lichen thallus surface. We generated a time-series of  $S_e$  for each experiment by scaling the instantaneous thallus mass between the initial (i.e., assumed saturated and maximum) and final (assumed residual) thallus masses, assuming that changes in mass reflect only changes in water content. From the time-series of evaporation rates observed in each desiccation experiment, we generated a time-series of vapor pressure differences between lichen surface and air by dividing by  $\beta$ . Next, we estimated a time-series of the vapor pressure of the lichen surface as the air's vapor pressure (calculated by Teten's (1930) equation using the measured air temperature and relative humidity) plus the aforementioned vapor pressure differences. A time-series of the relative humidity of the lichen surface was calculated by dividing the lichen surface's vapor pressure by the saturated vapor pressure. The matric potential of the lichen surface was calculated by inversion of Eqn 2. Lastly, we plotted the estimated matric potentials against the effective saturations and fit a modified logistic function to the data from a single drying experiment, namely the experiment performed under 0.34 RH. We chose the 0.34 RH experiment as the sole data set for parameterizing the model because 0.34 RH was the driest air humidity we tested, thereby spanning the largest range of water potentials for the lichen for which the final water content likely best represented the thallus' residual water content, and so that we could use the remaining desiccation experiments for model validation. Our fitting function is an asymptotic equation between 0 and 1, modified from the logistic function, and defined as

$$S_e = \left( \frac{1}{1 + \exp(-a(\psi_m - b))} \right)^c \quad (3)$$

where  $a$  [ $\text{m}^{-1}$ ],  $b$  [m], and  $c$  [-] are the fitting parameters. After performing logarithmic transformations on  $S_e$  data from the 0.34 RH

experiment, we observed piece-wise behavior with two distinct regions for  $S_e > \sim 0.55$  and  $S_e < \sim 0.55$ , each with their own logarithmic-slopes. Consequently, we defined the  $a$  parameter as a piece-wise function of matric potential ( $a = a_1 + (a_2 - a_1)H(\psi_m - b)$ , where  $H(x)$  is the heavy-side step function). The physical meaning of  $b$  is the matric potential at which the two piecewise regions intersect, and  $0.5^c$  is the effective saturation at  $\psi_m = b$ . Despite having a piece-wise  $a$  parameter, our fitting function for  $S_e$  is continuous. However, its derivative with respect to matric potential is discontinuous at  $\psi_m = b$ . We removed the discontinuity in  $\partial S_e / \partial \psi_m$  by Gaussian smoothing of the fit for  $S_e$  over a 200 m standard deviation.

This method reflects only the bulk retention of all water and does not distinguish between internal and external water or water stored in different morphological layers. It also assumes that the vertical water potential profile is relatively uniform such that the matric potential at the top and bottom surfaces (i.e., where evaporation was calculated) approximates the matric potential elsewhere in the thallus (since the measured thallus mass content considers the entire thallus). This is reasonable considering the high hydraulic conductivity of bulk lichen (Voortman et al., 2014) relative to thallus thickness that enables near vertically homogenous water potentials. There likely exists a water potential gradient between fungus and algae; however, this gradient does not invalidate our method, because the algae represent a far smaller water storage than do the fungus who's water potential controls evaporation at the cortices.

### 3 | MODEL DESCRIPTION

Our approach assumes that lichen media can be modeled as multiple, separate compartments for water storage, each capable of having distinct hydraulic and mechanical properties, similar to multiple-porosity models of other porous media (e.g., Gerke & van Genuchten, 1993). We conceptualize lichen as a multiple-porosity, swelling porous media system comprised of three main compartments for water storage: (1) fungal filaments that store liquid water, (2) algae that store liquid water and exist solely within the photobiont layer, and (3) the variably saturated extracellular pore-space between bundles of filaments and cells that contains both liquid water and vapor. Adopting the terminology of Eriksson et al. (2018), fungal filaments and algae cells both represent stores for "internal" water, while the liquid water and vapor in the extracellular pore-space represents the "external" water that suppresses photosynthesis when supersaturated by slowing diffusion of gasses to the photobiont (Green et al., 2011; Lange et al., 1993,

2001). We conceptualize the fungal and pore storages as vertically continuous domains that are laterally differentiated from one another and which span the four main morphological layers (upper cortex, photobiont layer, medulla, and lower cortex), bound between the interfaces of lichen, atmosphere, and the substrate below. The algal compartment exists within a continuous, vertical domain defined by the bounds of the photobiont layer that are specified within the model by the user.

Figure 1 illustrates the spatial distribution of each water storage in our conceptual model and the various paths for water exchange. Fluxes of water within the thallus and between the thallus and its environment are governed by physical laws of fluid-potential driven flow, namely, the motion of liquid water and vapor are described by Darcy's law and Dalton's law, respectively (Eqns S23–S27 and S.30 in Supporting Information). We define “vertical” flow as the flow within a compartment and “horizontal” flow as the flow between compartments. Liquid water and vapor flow “vertically” between pores of different morphological layers with flow-rate,  $q_{w,P}$  [ $\text{m s}^{-1}$ ], and interact directly with atmosphere above and substrate below through evaporation rates,  $E_{P,top}$  and  $E_{P,bottom}$ , respectively [ $\text{m s}^{-1}$ ]. Similarly, liquid water flows “vertically” between fungal filaments of different morphological layers with flow-rate,  $q_{w,F}$  [ $\text{m s}^{-1}$ ], and interact directly with atmosphere above and substrate below through evaporative-rates,  $E_{F,top}$  and  $E_{F,bottom}$ , respectively [ $\text{m s}^{-1}$ ]. The hydraulic conductivity associated with  $q_{w,P}$  is treated empirically as a function of external water content (Voortman et al., 2014). The conductivity linked to  $q_{w,F}$  is estimated from the Hagen–Poiseuille equation and the filaments' radii and modified by a pore-factor to account for the resistance related to septal pores between fungal cells (Sanders & Ríos, 2017). The pore-factor was originally derived by Thompson and Holbrook's (2003) to describe the resistance of sieve plates within the phloem of higher plants. “Horizontal” flows between compartments are represented by lateral transfer terms ( $\Gamma_{w,1}$ ,  $\Gamma_{w,2}$ ,  $E_1$ ; Gerke & van Genuchten, 1993). The pores and the fungal filaments communicate through two transfer terms:  $\Gamma_{w,1}$  which describe liquid water flow [ $\text{m s}^{-1}$ ], and  $E_1$ , which describes the unidirectional, evaporative loss of water from the fungal filaments to pores [ $\text{m s}^{-1}$ ] when the vapor pressure within pores is less than that of fungal filaments. We chose  $E_1$  to be unidirectional because water may evaporate from fungus to pore when the vapor pressure of the pore is less than that of the fungus, however, when the vapor pressure of the pore is greater than that of the fungus, water can condensate from vapor in the pore-space on the filaments' external surfaces and later infiltrate. Fungal filaments and algae cells communicate solely in the photobiont layer through a second liquid water transfer term,  $\Gamma_{w,2}$  [ $\text{m s}^{-1}$ ], that represents the passive flux of water conducted through mycobiont–photobiont interfaces, including hyphae and intragelatinous protrusions (Honegger, 1991, 2006). We chose not to allow algae to communicate directly with pores because photobionts wall surfaces are coated with and sealed by mycobiont-derived hydrophobic compounds (Honegger, 1984, 1991, 2006), and we hypothesize that algae communicate indirectly with pores through the intermediary fungal filaments. The hydraulic conductances associated with both  $\Gamma_{w,1}$  and  $E_1$  act over the entire surface area of fungal

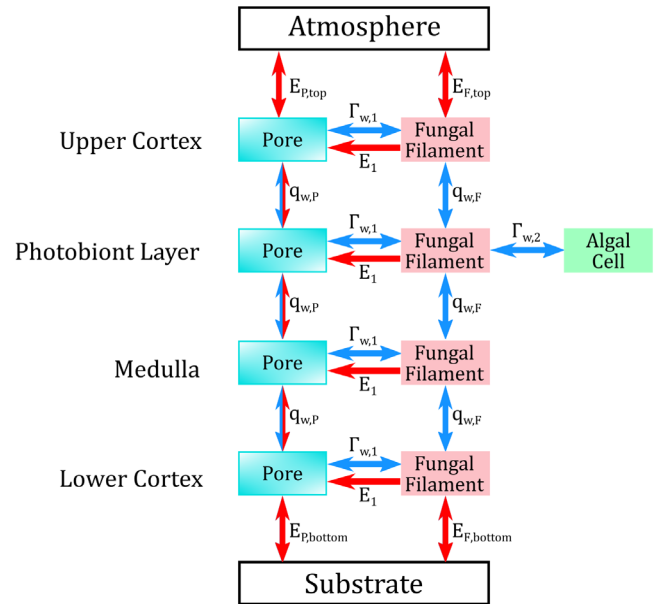


**FIGURE 1** Pathways for water transport between three compartments: fungal filaments, algae cells, and the extracellular pore-space between them. Liquid water and vapor flow “vertically” between pores with flow-rate,  $q_{w,P}$  [ $\text{m s}^{-1}$ ], and interact directly with atmosphere above and substrate below through evaporation rates,  $E_{P,top}$  and  $E_{P,bottom}$ , respectively [ $\text{m s}^{-1}$ ]. Similarly, liquid water flows “vertically” between fungal filaments with flow-rate,  $q_{w,F}$  [ $\text{m s}^{-1}$ ], and interact directly with atmosphere above and substrate below through evaporative-rates,  $E_{F,top}$  and  $E_{F,bottom}$ , respectively [ $\text{m s}^{-1}$ ] during wetting and drying. The pores and the fungal filaments communicate through two transfer terms:  $\Gamma_{w,1}$  which describes liquid water flow [ $\text{m s}^{-1}$ ], and  $E_1$ , which describes the unidirectional, evaporative loss of water from the fungal filaments to pores [ $\text{m s}^{-1}$ ] when the vapor pressure within pores is less than that of fungal filaments. Fungal filaments and algae cells communicate solely in the photobiont layer through the  $\Gamma_{w,2}$  liquid water transfer term [ $\text{m s}^{-1}$ ]. Blue arrows represent fluxes of liquid water, and red arrows represent fluxes of water vapor ( $q_{w,P}$  may represent liquid and/or vapor water flow depending on the degree of saturation)

filaments. The conductance of the former is estimated as that of the filaments' cellular membrane, and the conductance of the latter is estimated from  $\beta$ , assuming that the thallus' internal resistance to vapor flow may be approximated by its surface resistance to vapor flow. The hydraulic conductance associated with  $\Gamma_{w,2}$  considers only the morphology of the mycobiont–photobiont interfaces and is estimated by the Hagen–Poiseuille equation from the interfaces' radii (see Supporting Information).

We introduce three major improvements upon earlier models to describe the hydration controlled swelling and shrinking of lichen: (1) we model water fluxes through physical laws (Darcy's and Dalton's laws), (2) we quantify the porosity and water content of lichen through the unitless measures of void-ratio,  $e$  (volume ratio of fluid to solid phases), and water-ratio,  $\vartheta$  (volume ratio of water to solid phases), respectively, and (3) we evaluate our model vertically through an alternative, porosity-less, compacted coordinate system referred to as the “material” coordinate,  $m$  (Philip, 1969; Smiles & Rosenthal,

1968), rather than a traditional, Cartesian vertical coordinate system,  $z$ , to simplify computation. The advantage is that the domain of the lichen thallus when converted to the material coordinate is static and defined between  $[0, M]$ , where  $M$  is the total compacted thallus thickness.  $M$  is a constant and does not change during swelling and shrinking. Alternatively, if we were to apply the Cartesian coordinate system, the domain of the lichen thallus would be defined as  $[0, Z(t)]$ , where  $Z$  is the true thickness of the thallus and changes over time,  $t$ , as the thallus swells and shrinks. Water-ratio and void-ratio are defined relative to the volume of solid phases within the lichen rather than total volume or mass. These measures of water and gas volumes agree with the paradigm of the material coordinate, since the compacted coordinate,  $m$ , depends only on the volume of solid phases as shown in Fig. 2. The model simulates wetting and drying of the lichen by calculating the change in water potential within a deforming, vertical domain in fungus, algae, and extracellular pore-space compartments simultaneously through fully explicit finite difference. The complete approach and mathematical equations employed here are described in Supporting Information, including explanation of our domain discretization and numerical solution in matrix terms.

We validate our model by comparing simulation results to observations from our desiccation and hydration experiments on *F. caperata*. We simulated multiple desiccation experiments on initially saturated thalli subjected to varying severities of water stress, each under constant boundary conditions corresponding to the water potentials produced during our laboratory desiccation experiments (between  $-92$  and  $-148$  MPa). We simulated thallus hydration for a thallus initially equilibrated to the laboratory's air water potential ( $0.21$  RH and  $26$  °C) subjected to boundary conditions based on the relative humidity and temperature measurements taken from inside the hydration chamber during our hydration experiment.

We apply our model to investigate our three questions: (1) Where is the bottleneck to water transport in the lichen thallus? (2) How do hydration and dehydration dynamics differ? and (3) What causes these differences? To test our first hypothesis that vapor transport between the air and the lichen at its cortices is the limiting step on how quickly bulk thallus water content equilibrates with its surroundings, we interpret the spatial distribution of matric water potentials within the thallus simulated during wetting and drying experiments. Uniformity in potentials within compartments suggests negligible internal resistance to water flow, while sharp gradients suggest considerable resistance. This hypothesis would be supported by findings of vertical water potential profiles within pore-space, fungal filament, and algae compartments. We interpret matric potential profiles throughout the duration of two drying experiments previously used to validate the model (drying experiments 1 and 4;  $0.34$  RH/ $25$  °C and  $0.51$  RH/ $22$  °C, respectively) and a new wetting simulation with constant boundary conditions ( $0.97$  RH/ $25$  °C) and initially in equilibrium with  $0.51$  RH and  $25$  °C.

To test our second hypothesis that the strong nonlinearities in the hydraulic capacitance of the lichen thallus govern the difference in the time-scales for wetting and drying, we compared the time-scales of wetting and drying experiments simulated with four water retention curves of varying nonlinearity. All simulations were performed at  $25$  °C and either began in equilibrium with  $0.57$  RH and

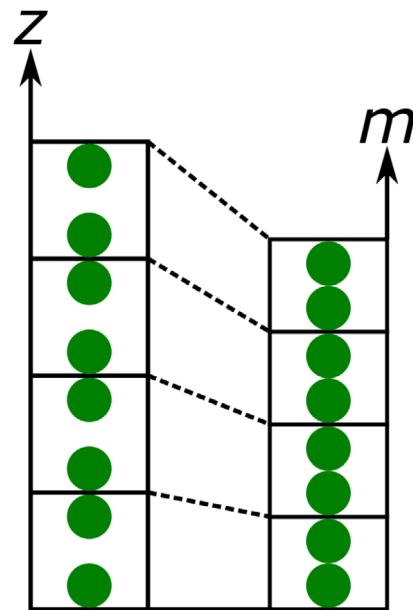


**FIGURE 2** Compacted, “material” coordinate,  $m$ , in relationship to traditional, Cartesian vertical coordinate,  $z$ . Green circles represent solid phases of matter. The traditional vertical coordinate,  $z$ , depends on the volume of all phases of matter within the system, while the material coordinate,  $m$ , depends solely on the volume of solid phases [Color figure can be viewed at [wileyonlinelibrary.com](http://wileyonlinelibrary.com)]

equilibrated with  $0.99$  RH (wetting) or vice versa (drying). All four retention curves intercept the same values of water content at the experimental limits in potentials ( $25$  °C;  $0.57$ – $0.99$  RH). The four retention curves include: (1) the  $S_e$ – $\psi_m$  relationship interpreted from measurement and fit to Eqn 3, (2) a purely linear function, (3) a function with muted nonlinearity, and (4) a function with exaggerated nonlinearity. These curves are shown later in Fig. 9a under the Results section. Functions with muted and heightened nonlinearities were created by normalizing the  $S_e$ – $\psi_m$  relationship interpreted from measurement between the bounds corresponding to  $0.57$  and  $0.99$  RH, which were chosen to represent a range of water potentials where lichen productivity may be limited by water stress, raising the normalized form by a factor ( $\frac{1}{2}$  and  $2$  for muted and heightened nonlinearities, respectively), and rescaling the new relationships between the proper bounds of water content. We forced osmotic potentials to zero in these simulations to ensure that the ranges of matric potentials were the identical. We determined the time for the lichen to equilibrate with its surroundings as the first simulated time that bulk lichen water content was within 98% of its equilibrium water content (both normalized by initial water content).

## 4 | RESULTS

### 4.1 | Estimation of lichen hydraulic properties

Regarding the aerodynamic conductance of vapor transfer between the surface of our *F. caperata* samples and the surrounding air, or the

parameter  $\beta$ , in Fig. 3, we report initial evaporation rates of bulk lichen measured in five desiccation experiments. As we expected, the evaporation's relationship with the vapor pressure difference is linear. This linearity reflects that Dalton's law (Eqn 1) describes the water loss from lichen with a conductance uniform among experiments. We fit the initial evaporation with a linear relationship with zero-intercept according to Dalton's law. The slope of this relationship,  $\beta$ , represents the bulk lichen's two-sided conductance to vapor flow, and we estimate the

value of  $\beta$  for our lichen samples as  $6.34 \times 10^{-3} \text{ mm day}^{-1} \text{ Pa}^{-1}$  ( $7.34 \times 10^{-11} \text{ m s}^{-1} \text{ Pa}^{-1}$ ). This conductance is a key parameter in our model that governs the rate of vapor flow through the top and bottom sides of the thallus, and we assume this conductance remains constant throughout desiccation and may reasonably describe evaporative vapor fluxes within the thallus between fungal filaments and surrounding extracellular pores (see Supporting Information). This latter assumption implies another underlying assumption that the resistance to vapor

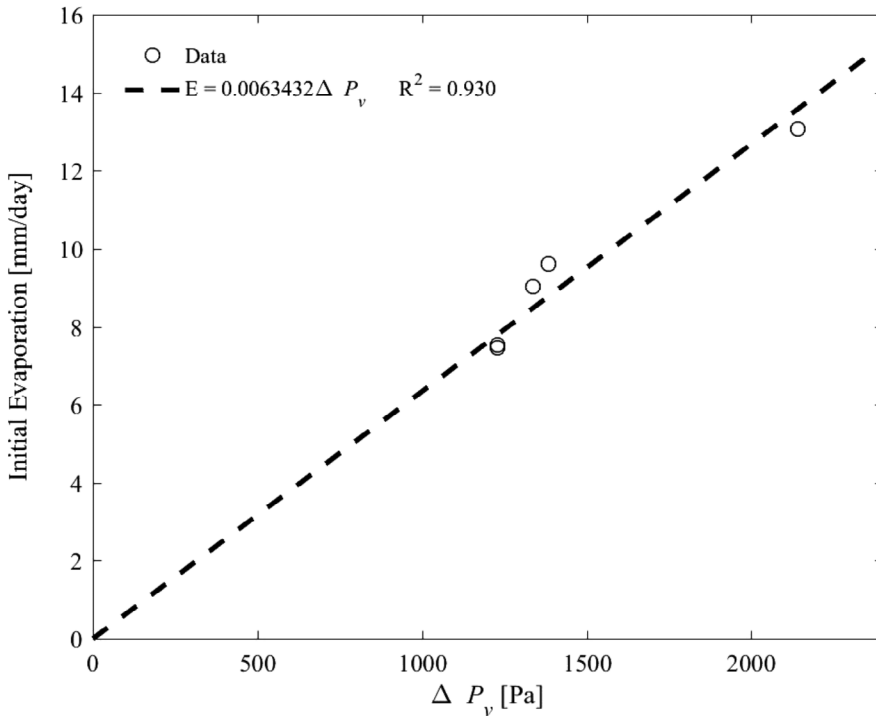


**FIGURE 3** Initial evaporation rate of bulk thallus during desiccation versus estimated vapor pressure difference. The dashed line represents the linear regression passing through the origin, and the slope of the dashed line is the two-sided (top and bottom) aerodynamic conductance to water vapor exchange between the lichen and the air

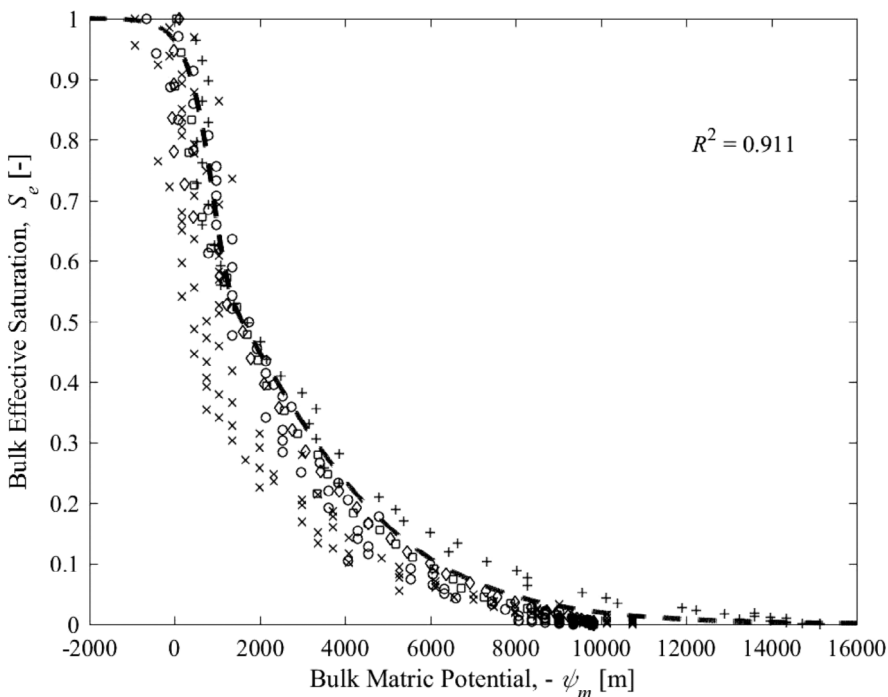


**FIGURE 4** Bulk thallus effective saturation (water content normalized between 0 and 1) versus estimated bulk thallus matric potential. Different symbols represent data from desiccation experiments, each with different atmospheric water potentials (plus signs are 0.34 RH and 25 °C, cross signs are 0.46 RH and 21 °C, squares and diamonds are both 0.49 RH and 20 °C, and circles are 0.51 RH and 22 °C). The dashed line is a modified logistic function (Eqn 3) fitted to data from only one desiccation experiment (0.34 RH, 25 °C, plus signs) and smoothed by a Gaussian filter with a 200 m standard deviation

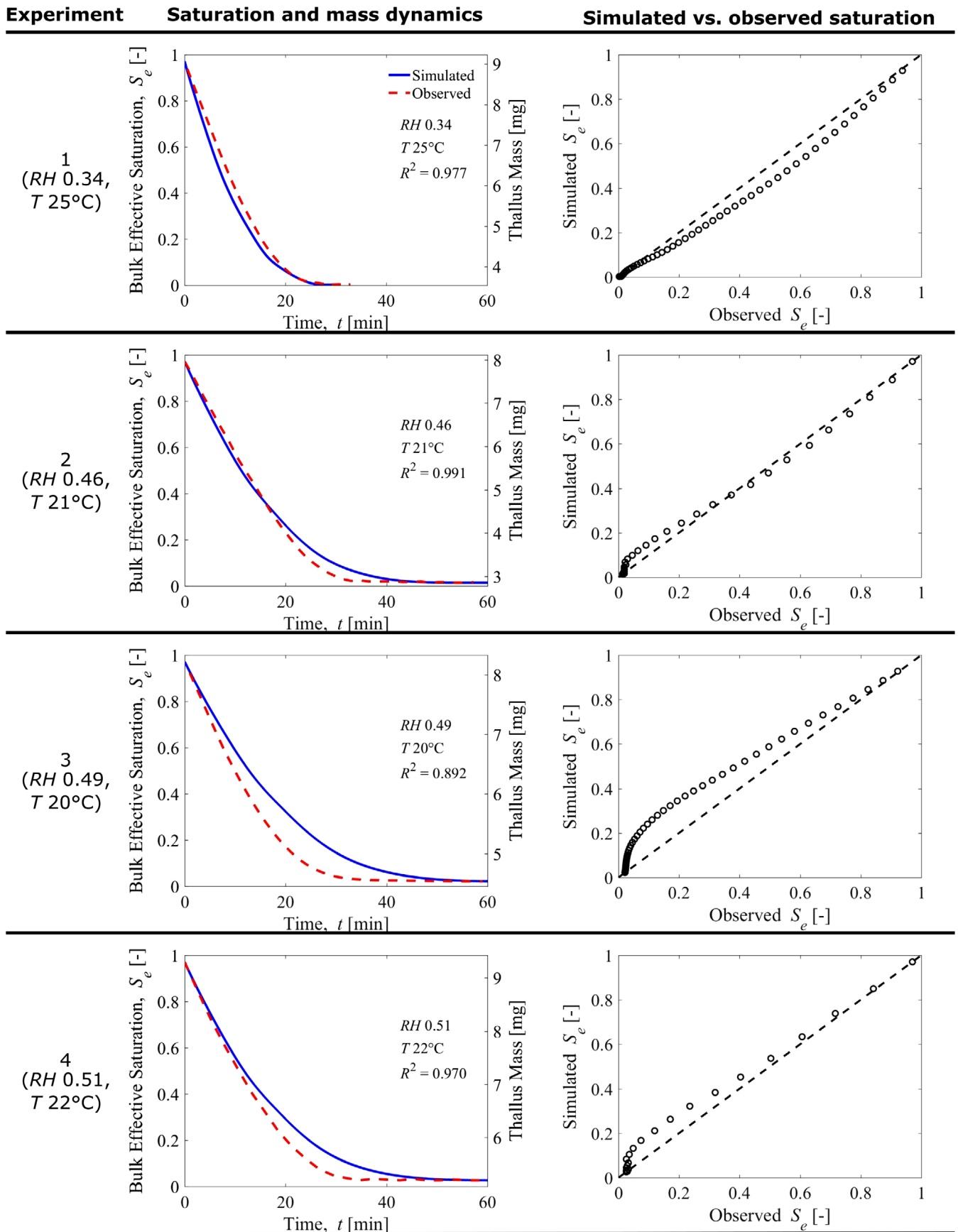


FIGURE 5 Legend on next page.

flow at thallus boundaries is dominated by contributions from the fungus rather than the pore-space, and consequently the bulk vapor resistance reasonably approximates the resistance to vapor transport across fungal walls. To test our assumption that  $\beta$  is relatively constant and insensitive to water content, we interpreted  $\beta$  again from the one hydration experiment. Though there are large uncertainties associated with our estimate of  $\beta$  during the wetting regime due to the hydration experiment's changing boundary conditions, all values between the 95th and 5th percentiles of the distribution of potential  $\beta$  values determined through a systematic permutation analysis range between  $\sim 1$  and  $\sim 3$  times the  $\beta$  interpreted from drying experiments, and the mean of potential  $\beta$  values estimated from wetting is  $\sim 2$  times the  $\beta$  interpreted from drying experiments (Fig. S2 in Supporting Information), suggesting that our assumption is relatively reasonable, considering that estimates of hydraulic conductances can vary over many orders of magnitude for soils and xylem of vascular plants between different hydration statuses (see Supporting Information for further discussion).

Regarding the functional relationship between saturation level and water potential that drives flow, when the effective saturation (water content normalized between 0 and 1) of bulk lichen is plotted versus the estimated bulk matric potential, a sigmoidal relationship is apparent in Fig. 4. We fit this relationship with a modified logistic function equation (Eqn 3) using data combined from a single desiccation experiment (0.34 RH, 25 °C) and applied a Gaussian filter with a 200 m standard deviation to smooth discontinuities in its first derivative. The coefficient of determination of the fit to the single desiccation experiment,  $R^2$ , is 0.912. This constitutive relationship represents the highly nonlinear, hydraulic capacitance of the lichen that is required in the model to relate between changes in water content and changes in water potential, the driving force for water flow. The shaping parameters of the fit (Eqn 3) shown in Fig. 4 are defined in Table 1.

## 4.2 | Model validation

We validated our model by comparing simulations or bulk thallus water content to measurements of thallus mass during desiccation of initially saturated *F. caperata* samples and during hydration of a sample initially equilibrated to 0.21 RH and 26 °C. We attempt to reproduce the dynamics of both water content and evaporation rate during drying as a test of the model's assumptions. We compare the evaporative response because it is a more difficult behavior to capture than water content and therefore a more sensitive measure for validation. For our hydration simulation, we compare simulations to observations for only water content and not evaporation because of significant

noise in the experimental thallus mass data. For the chamber's high relative humidity to wet the lichen sample, we had to remove the gravimeter's cover that is otherwise intended to prevent vibrations and other disturbances outside of the chamber from creating noise in the gravimeter's readings.

Figure 5 reports our simulated results of bulk effective saturation,  $S_e$ , (also expressed as bulk thallus mass) of initially saturated lichen drying under exposure to dry air (RH 0.34–0.51) and comparison of simulated and observed saturations. We performed five laboratory experiments, used one for parameter calibration and performed validation simulations for three of the four remaining experiments, because two desiccation experiments repeated the same environmental temperature and relative humidity (T 20 °C; RH 0.49). Simulations agree well with measurements ( $R^2$  between 0.892 and 0.991), with best agreement at the wet beginning of simulations. When approaching the driest lichen state, our model overpredicts the duration of the hydrated period, particularly in experiments with  $RH \geq 0.46$  (experiments 2–4 in Fig. 5). Figure 6 reports our simulated results of bulk two-sided evaporation,  $E$ , for the same simulations as shown in Fig. 5 and comparison with measurements. Predictions of evaporation rate also agree well ( $R^2$  between 0.811 and 0.982), but unlike water content before, there is no general trend for when simulated evaporation agrees best with observations.

Figure 7 shows the model and inputs and results of our hydration simulation in comparison to observations. For this simulation, we defined the model's boundary conditions from the relative humidities and temperatures measured inside the hydration chamber. The model requires a continuous input of relative humidity and temperature values to determine boundary conditions, and so we fit log-linear equations ( $y = A \cdot \ln[x + 1] + B$ ) to relative humidity and temperature measurements and defined the model's boundary conditions from the fits. Despite significant noise in the gravimeter measurements from having removed the gravimeter's cover (discussed above), simulations and observations of hydration agree well ( $R^2$  of 0.726), particularly considering that the model parameters that we estimated from laboratory data ( $\beta$  and  $S_e[\psi_m]$ ) came from inversion of a single desiccation experiment.

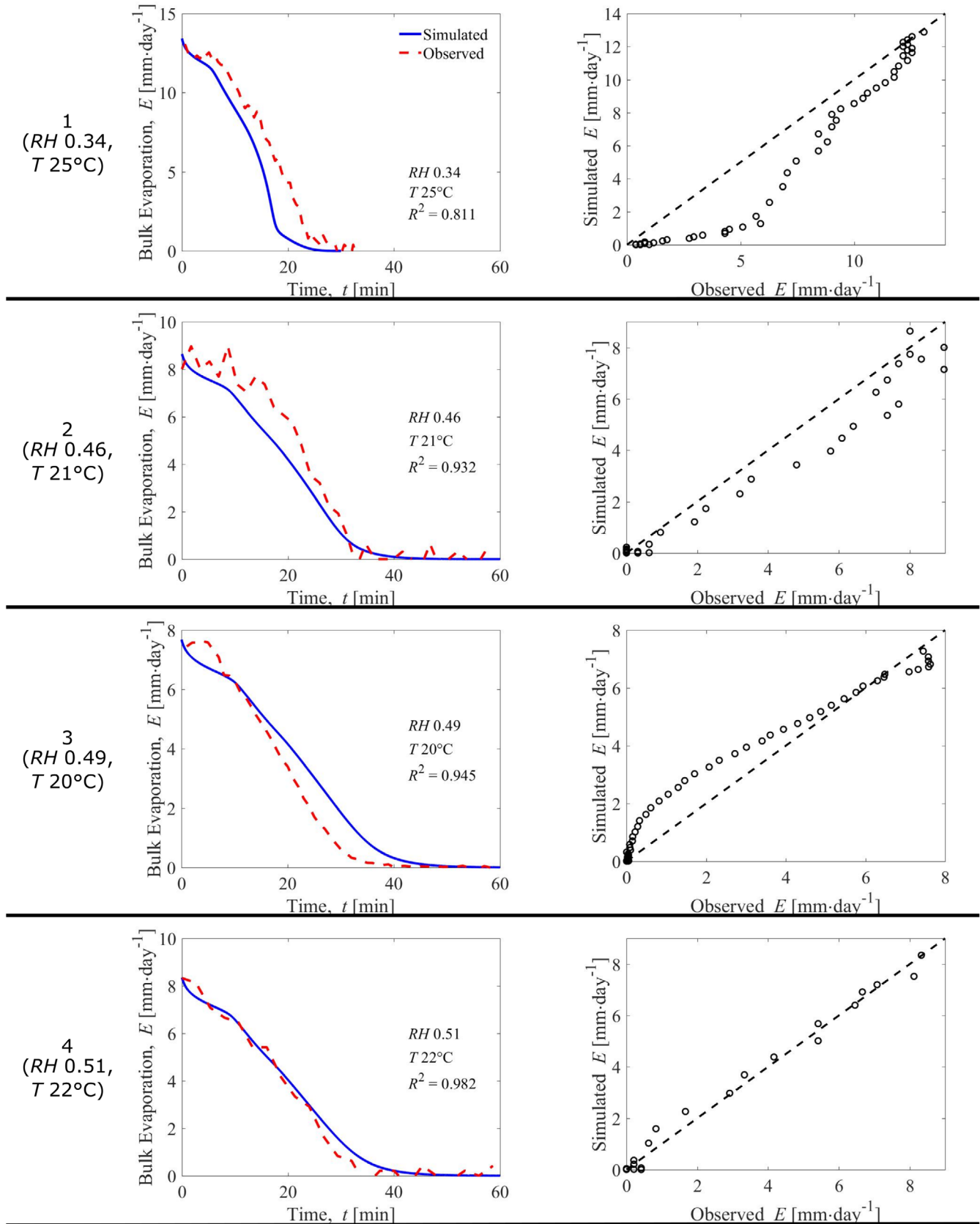
## 4.3 | Hydraulic gradients and resistances

Figure 8 shows the distribution of matric potentials within the thallus during two drying experiments (initially saturated; experiments 1 and 4 in Figs. 5 & 6) and a wetting experiment with constant boundary conditions (0.97 RH; 25 °C) and initially in equilibrium with 0.51 RH and 25 °C. We consider two drying experiments with different

**FIGURE 5** Comparison of measured and simulated thallus saturation. Data is presented by row to differentiate environmental conditions and by column to differentiate results. The left column shows simulated and observed dynamics of thallus moisture expressed by both bulk effective saturations,  $S_e$ , and total masses; solid blue lines represent simulations, and dashed red lines represent observations. The right column presents a comparison of simulated and observed effective saturation (open circles); the dashed line in each plot is the theoretical optimal 1:1 fit between simulations and observations. Note that experiment 1 was used for parameter fitting, and experiments 2–4 are model validations [Color figure can be viewed at [wileyonlinelibrary.com](http://wileyonlinelibrary.com)]

**Experiment Two-sided evaporation dynamics**

**Simulated vs. observed evaporation**



**FIGURE 6** Legend on next page.

boundary conditions to ensure that the trends in potentials were independent of the rate of thallus evaporation. As hypothesized, matric potentials are near uniform within each compartment (pore-space, fungal filaments, and algae) but varied among compartments in both wetting and drying simulations, meaning that potentials equilibrate faster within a compartment than among compartments or with the bounding air. The uniform potential profiles confirm the assumption made in our inverse-modeling of model parameters from observations (water retention and capacitance) and suggest that vertical resistances are negligible within the thallus (between cortices, photobiont layer, and medulla), while the sharp gradient in potentials near the surface of the cortices suggest that the vertical resistance to water flow are concentrated at the sites of vapor transport between lichen and the atmosphere, supporting our first hypothesis. These results also support earlier models that simulate lichen bulk moisture dynamics and model vapor dynamics at the cortices as the dominant control on hydration and desiccation (Jonsson et al., 2008; Paterson et al., 1983; Péch, 1989). However, these earlier models cannot describe the internal gradients between symbionts and external water.

The greatest difference in water potentials between compartments occurred between fungus and pore-space. This gradient is initially small, grows during wetting and drying, peaks, and then declines as equilibrium is approached (Fig. 8). The hydraulic gradient between fungus and pore-space suggests that the mycobiont equilibrates with the atmosphere slower than extracellular, external water and that the pore-space wets and dries faster than the filaments, thereby controlling the periods for optimal gas transfer within the thallus that support photosynthesis and respiration. Our simulations were performed with the same vapor conductance,  $\beta$ , and same water retention curves applied to both fungus and pore-space compartments, so these response dynamics reflect differences in the internal structure of pore-space and fungal filaments. Pore-space and filaments differ in geometry and in their relative contribution to the total thallus volume. In the model, filaments are cylindrical, while pores are amorphous (assumed to describe their surface areas and deformability; Eqns S.29, S.31, and S.33), and their volumetric contributions are represented by different weights ( $w_F$ ,  $w_A$ ,  $w_P$ ; Table 1). The phenomenon of pores desaturating faster than fungal filaments occurs in reality and is typically associated with hydrophobic surfaces inside the thallus that support gas transport (Honegger, 1991; Lidén et al., 2010). However, our model does not currently describe these additional effects of hydrophobicity and would require applying different water retention curves to fungus and pore-space. The inclusion of more hydrophobic pore-space in the model would amplify the hydraulic gradient between mycobiont and external, extracellular water. Additionally, these internal gradients do not invalidate the notion of small internal resistances

to the lichen's bulk moisture status, because pore-water represent a small fraction of lichen's water available for transport (represented by weights,  $w_F$ ,  $w_A$ ,  $w_P$ ; Table 1).

The difference in potentials between fungus and algae was relatively smaller than between pore-space and fungus (Fig. 8), emphasizing both the symbiosis between mycobiont and photobiont and the mycobiont's ability to prolong hydration against a quickly drying pore-space. Generally, the hydraulic gradient between fungus and algae peaked early and then rapidly declined during drying, while the gradient remained relatively constant throughout wetting. We believe that this hydraulic gradient may play a critical role in lichen symbiosis by controlling the transport of nutrients, sugars, and carbohydrates between mycobiont and photobiont. Wetting would aid transport of nutrients from mycobiont to photobiont, while drying would aid transport of sugars and carbohydrates from photobiont to mycobiont. Additionally, our results that potentials are not constantly uniform between fungus and algae may partially explain the time-lag between the onset of bulk lichen saturation and the turning on of photosynthesis (Jonsson-Čabrajić et al., 2010; Lidén et al., 2010). Bulk saturation best represents the moisture status of the mycobiont, since it makes up most of the thallus, while photosynthetic potential depends only on the hydraulic status of the photobiont. We show here that the hydration statuses of mycobiont and photobiont differ. In future work, we aim to investigate whether this disconnect could be a control on the activation time for photosynthesis during wetting and drying.

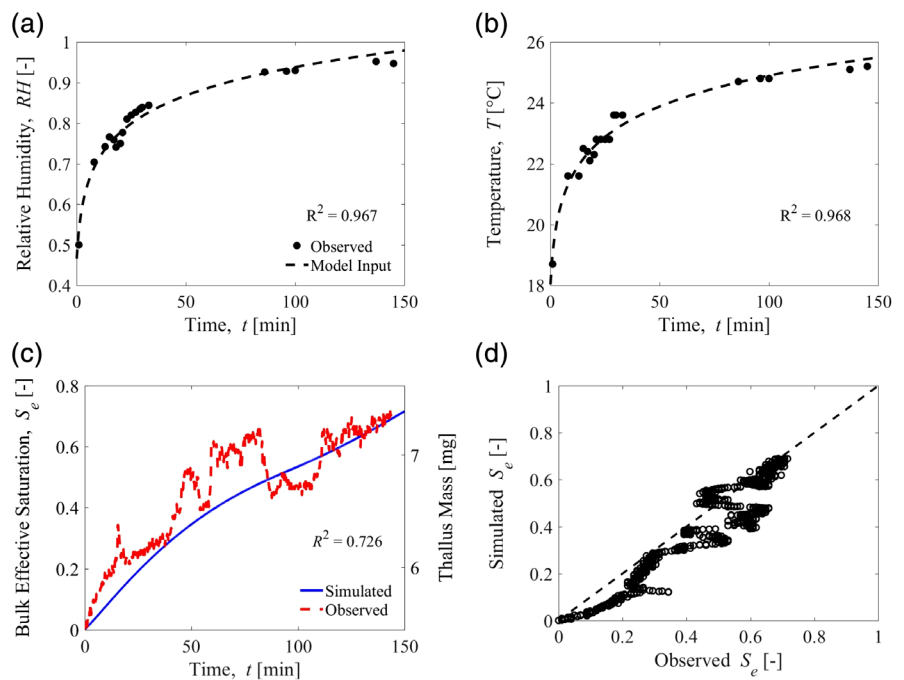
#### 4.4 | Nonlinearity in hydraulic properties control time scales of hydration and desiccation

Figure 9a shows the four water retention curves of varying nonlinearity that we created and applied to our model to investigate the role of strong nonlinearities in the hydraulic capacitance on the difference in the time-scales for wetting and drying. The purely linear function result in a constant capacitance throughout changes in moisture. For each of the three nonlinear curves, capacitance is largest in the wet regime (meaning the water storage is highly responsive to water fluxes) and approaches zero in the dry (meaning water storage is less responsive). We quantify the nonlinearity of our curves through relative nonlinearity,  $\lambda$  (Emancipator & Kroll, 1993), which is defined as the root mean square of the deviation of a function from an ideal straight line normalized by the span along the x-axis. The linear retention curve (red line in Fig. 9a) has a relative nonlinearity of 0% by definition, while the relative nonlinearity of the most nonlinear curve (blue line in Fig. 9a) is 0.17%. The degree of nonlinearity governs how

**FIGURE 6** Comparison of measured and simulated thallus evaporation. Data is presented by row to differentiate environmental conditions and by column to differentiate results. The left column shows simulated and observed dynamics of two-sided thallus evaporation,  $E$ ; solid blue lines represent simulations, and dashed red lines represent observations. The right column presents a comparison of simulated and observed evaporation rates (open circles); the dashed line in each plot is the theoretical optimal 1:1 fit between simulations and observations. Note that experiment 1 was used for parameter fitting, and experiments 2–4 are model validations [Color figure can be viewed at [wileyonlinelibrary.com](http://wileyonlinelibrary.com)]



**FIGURE 7** Validation of model under wetting regime. (a) Measured relative humidity and (b) temperature (black circles) within hydration chamber over the course of wetting experiment. The model requires a continuous input of relative humidity and temperature values to determine boundary conditions, and so we fit log-linear equations (dashed lines) to measurements that were used to define model boundary conditions. (c) Comparison of measured (dashed red line) and simulated (solid blue line) thallus saturation, expressed as both bulk effective saturations,  $S_e$ , and total mass. Significant noise in the gravimeter measurements of thallus mass arose from having removed the gravimeter's cover to allow vapor to enter the chamber. (d) Comparison of simulated and observed effective saturation (open circles); the dashed line is the theoretical optimal 1:1 fit between simulations and observations [Color figure can be viewed at [wileyonlinelibrary.com](http://wileyonlinelibrary.com)]



capacitance varies between wet and dry regimes. Increasing non-linearity causes a relatively larger capacitance in the wet state and a relatively smaller capacitance in the dry state. It is important to note that it is possible to generate alternative curves of heightened non-linearity with the opposite trend: lower capacitance in the wetter state and higher capacitance in the drier state. These curves would plot above the black line in Fig. 9a rather than below. However, this experiment was designed in part to consider the water-limitations to lichen productivity. Despite that these alternative curves would produce unique wetting and drying temporal responses, interpreting their results toward lichen productivity would be muddled, since these curves would suggest productivity maintained over a wide range of the simulated water potentials.

Generally, a larger capacitance helps to prolong periods of hydration; however, exactly how long that the wet period is prolonged depends on how the capacitance varies in time and as a function of water potential. We found that weak nonlinearity in capacitance (strong linearity) best prolonged the hydrated duration (drying time; Fig. 9b). Additionally, a more linear curve means greater water storage for a given potential and likely requires a more retentive and costly tissue with the stiffness to better retain water under tension. Because the curves in Fig. 9a were not created in a way that normalizes variations in the magnitude of capacitance among curves, we compare the ratio of times to wet and dry rather than solely the magnitude of times. Figure 9b shows that more nonlinear water retention curves caused longer times to wet from an initially dry state and shorter times to dry from an initially wet state. For the water retention curve fitted to observations (black line,  $\lambda = 0.11\%$ ), the duration of wetting was  $\sim 4$  times that for drying (Fig. 9b) in agreement with earlier studies reported in the literature (Jonsson et al., 2008; Jonsson-Čabrajčić et al., 2010). This ratio between wetting and drying times was

larger for more nonlinear water retention curves and ranged between 0.65 for the purely linear and 5.90 for the exaggerated nonlinear curve. The model's sensitivity to nonlinearities in the hydraulic capacitance of the lichen thallus supports our second hypothesis.

Since lichen's photosynthesis depends on its hydration status (Dahlman & Palmqvist, 2003; Palmqvist & Sundberg, 2000), neither long wetting times nor short drying times are advantageous for maintaining photosynthesis. Our results suggest that the purely linear water retention curve would be optimal for lichen's productivity (small wet-to-dry time ratio). In this sense, the water retention curve we measured from our *F. caperata* samples is not optimal (large wet-to-dry time ratio). We hypothesize that this suboptimality may be reconciled by considering the wet environment of *F. caperata* and the costs associated with developing stiffer, more retentive tissues. *F. caperata* is hygrophytic and tends to occupy humid areas (Incerti & Nimis, 2003; Giordani & Incerti, 2008), which allows them to maintain productivity consistently without the need to prolong internal moistures due to small environmental fluctuations with stable sources for moisture. *F. caperata*'s water retention may also be explained by a strategy that balances maintaining hydration and productivity during dry periods with the costs associated with the tissue responsible for the prolonging hydration. These costs of developing denser, stiffer tissues include increased respiration (Kytoviita & Crittenden, 2002), reduced light absorption (Crittenden, 1991), and the carbon and nutrient costs of growth which are costlier for denser, stiffer tissues. When these additional costs are considered, *F. caperata*'s water retention behavior may be optimal with regards to its environment. Our study is limited to the foliose-form lichen, particularly *F. caperata*, and their internal structure; however, there is great potential to adopt the same modeling philosophy to other lichen forms and structures to investigate how other lichens have adapted to the hydrology of their environments.

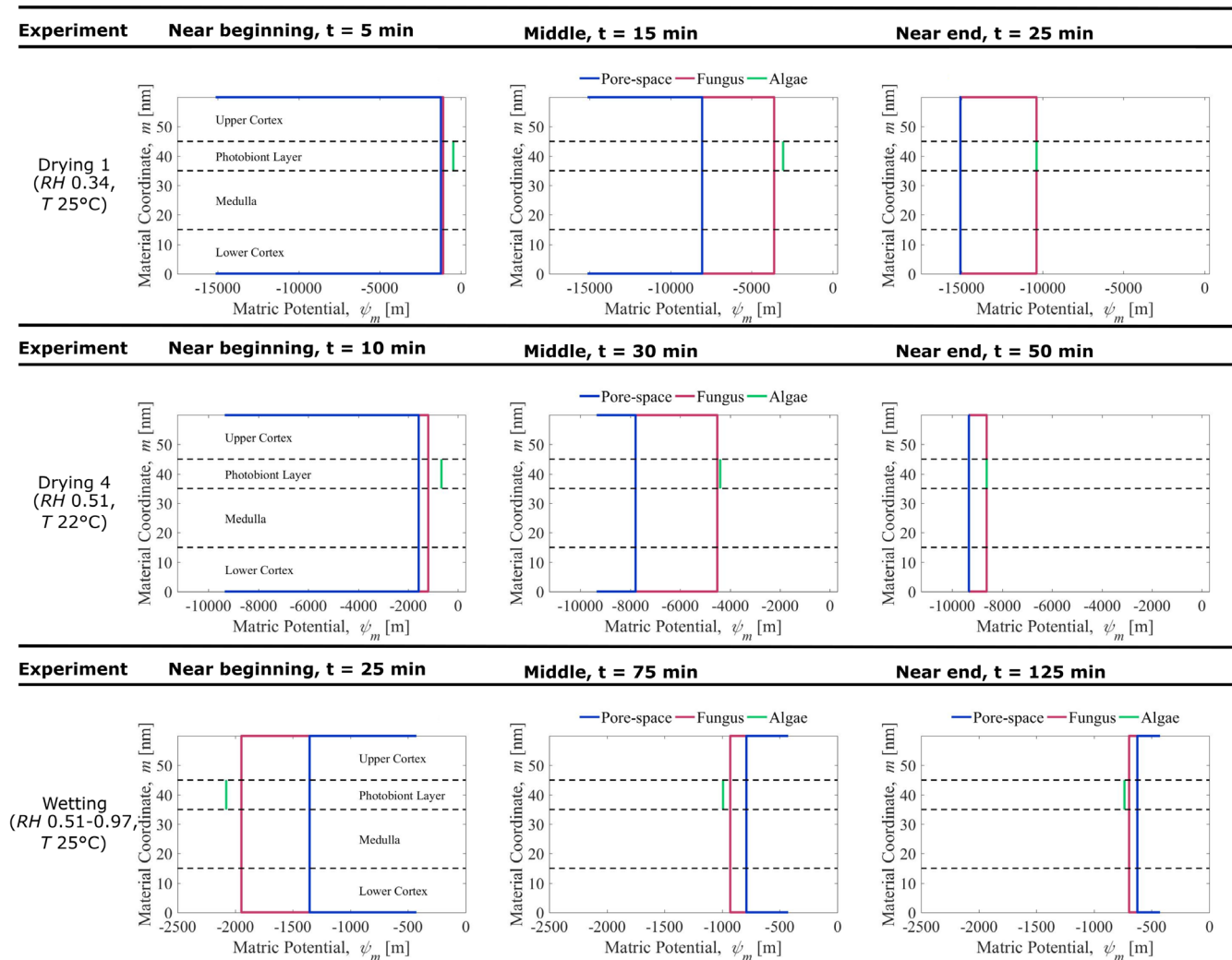


**FIGURE 8** Vertical matric water potential profiles within lichen thallus throughout duration of previous drying simulations (initially saturated; Figs. 5 & 6) and a new wetting experiment with constant boundary conditions (0.97 RH; 25 °C) and initially in equilibrium with 0.51 RH and 25 °C. Matric potentials are near within each compartment (pore-space, fungal filaments, and algae) throughout both wetting and drying, suggesting that vertical resistances are negligible within the thallus. Sharp gradients in matric potential at the boundaries suggest that vertical resistances are concentrated at sites of evaporation/condensation. Horizontal differences in matric potential between compartments represent the magnitude of resistance for water transport between compartments. Dashed lines represent the boundaries between morphological layers [Color figure can be viewed at [wileyonlinelibrary.com](http://wileyonlinelibrary.com)]

## 5 | DISCUSSION

Our model predicts well the dynamics of bulk lichen water content without relying heavily on empiricisms (Fig. 5). It describes the hydration controlled swelling and shrinking of lichen by explicitly representing the transport of water within the thallus, between mycobiont and photobiont, and between thallus and surroundings by physical laws of fluid mechanics (Darcy's law and Dalton's law). To our knowledge, it is the first attempt to describe the dynamic, spatial distribution of water within the thallus between symbionts and extracellular pores, while past models of lichen moisture describe a single water content for the entire thallus (Jonsson et al., 2008; Lloyd, 2001; Paterson et al., 1983; Péch, 1989). We believe describing the internal moisture distributions is an essential first step toward a mechanistic understanding of lichen photosynthesis.

Model predictions of both water content and evaporation during desiccation and hydration agree well with measurements for all samples, independent of hydration state (Figs. 5 & 7). However, further improvements can be made. Currently, osmotic potentials were assumed constant. We plan to explicitly model the concentration of osmolytes, particularly sucrose as in phloem models (e.g., Thompson & Holbrook, 2003), and preliminary tests suggest that this addition will improve estimates of both water content and evaporation. For simplicity, we assumed homogenous hydraulic and mechanical properties across the lichen thallus and applied a single relationship between the average water content and water potential to describe the pressure-volume relationships of each compartment (fungus, algae, and pores). However, the structure and composition of the lichen thallus is heterogeneous (De los Ríos, Ascaso, & Wierzos, 1999; Honegger & Peter, 1994), and we believe our assumed homogeneity is a coarse

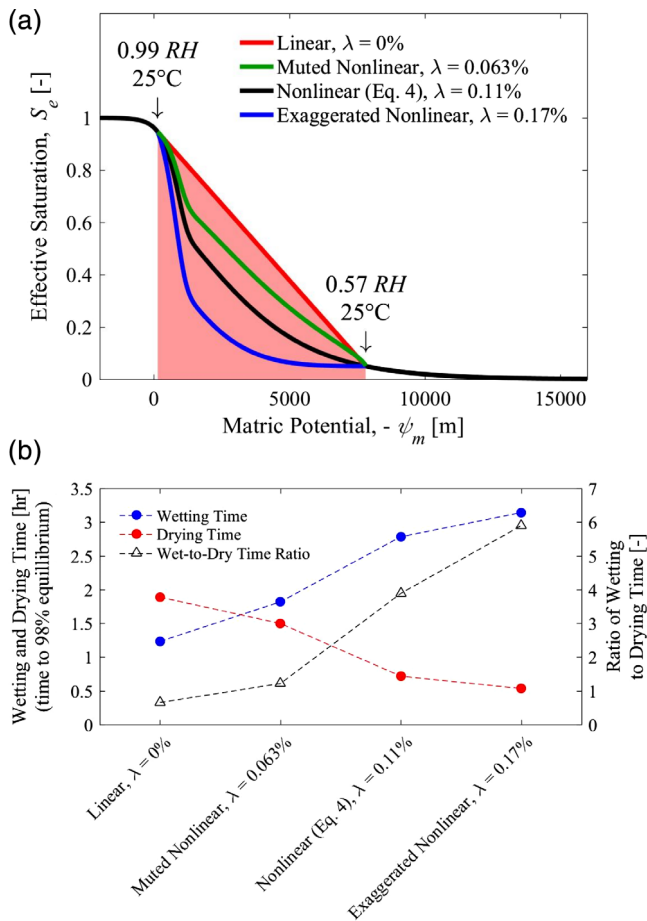


**FIGURE 9** Influence of nonlinearity in water retention and hydraulic capacitance on simulated thallus wetting and drying times. We compare the time to reach 98% of equilibrium for four different water retention curves (defined in terms of effective saturation,  $S_e$ ) of varying degrees of nonlinearity (denoted by relative nonlinearity,  $\lambda$ , defined by Emancipator & Kroll, 1993) during wetting and drying simulations. All simulations performed at 25 °C and either began in equilibrium with 0.57 RH and equilibrated with 0.99 RH (wetting) or vice versa (drying). (a) Four water retention curves used in analysis. The black curve is identical to the curve in Fig. 4 that was fit to measurements. The pink region shows the range of matric water potentials spanned in all simulations. We forced osmotic potentials to zero in these simulations to ensure that the ranges of matric potentials were identical. (b) Times to wet or dry and the wet-dry time ratio for each water retention curve [Color figure can be viewed at [wileyonlinelibrary.com](http://wileyonlinelibrary.com)]

approximation. There exist laboratory methods to estimate the hydraulic and mechanical properties of fungus, algae, storages of external water, and their interfaces. We summarize these methods as:

- Volume–pressure relationships (void-ratio and water-ratio) of individual fungus and algae cells can be developed similar to how others have measured the osmotically driven expansion of guard cells in higher plants (Franks et al., 1995; Franks, Cowan, & Farquhar, 1998; Meidner & Edwards, 1975; Zimmermann & Steudle, 1975).
- Eriksson et al. (2018) have distinguished between contributions of internal (fungus and algae) and external (extracellular pore-space)

compartments, which may allow for development of pressure–water content relationships of the pore-space component in the model.

- Ten Veldhuis et al. (2017) have differentiated between the evaporation rates of top and bottom surfaces of the thallus by sealing ends with tape. We believe this method can be extended to interpret each side's bulk conductance to water vapor.
- If the vapor conductance of nonlichenized fungal filaments can be determined experimentally, then the conductance of pores can be estimated as the difference in bulk lichen and fungal conductances. Both conductances are key parameters within our model.
- The dynamics of water transport between algal and fungal symbionts could be quantified by integrating microfluidic devices with (confocal) microscopy techniques. These techniques may improve estimation of the conductance of the mycobiont–photobiont interface. The challenge here, however, is to obtain dynamic imaging of a moving medium, as it is swelling and shrinking.

Future research will investigate the role of hydration dynamics on lichen metabolism and study the possibility of symbiotic gas exchange between photobiont and mycobiont. We aim to integrate gas transport into the model along with sink terms reflecting respiration and photosynthesis with the latter based on a Farquhar-type model (Farquhar et al., 1980) with modifications to describe the turning off of photosynthesis under highly negative water potentials (Vico & Porporato, 2008) or excess sugar concentrations (Hölttä et al., 2017). We will address the following questions: (1) To what extent are  $\text{CO}_2$  and  $\text{O}_2$  recycled between mycobiont and photobiont within lichen? (2) What are the time-scales over which lichen oversaturation restricts gas transport and ultimately suppresses photosynthesis?

## 6 | CONCLUSION

We present a mechanistic model to describe dynamic water transport within the lichen thallus, between mycobiont and photobiont, and between lichen and its surroundings based on physical laws and an approximate, compartmentalized architecture. We applied the model to test two hypotheses: (1) that vapor transport between the atmosphere and the lichen at its cortices is the dominant control on how quickly bulk thallus water content equilibrates with its surroundings, and (2) that the difference in the time-scales for wetting and drying are a product of the strong nonlinearities in the hydraulic capacitance of the lichen thallus. During drying, lichens resist negative potentials and prolong their hydrated, active periods through large resistances to vapor flow that are concentrated at the lichen's cortices, supporting our first hypothesis. Simulated near-uniform vertical water potential profiles within each water storage compartment (fungus, algae, and pore-space) suggest that the lichen's internal hydraulic resistances are small, emphasizing the role of cortical resistances to vapor flow on slowing desiccation and prolonging productivity. Water potentials are not uniform between mycobiont and photobiont or between mycobiont and extracellular water, and the deviation in water

potentials change dynamically throughout wetting and drying. These differences in water potential may serve as the driving force for transport of solutes (sugars and nutrients) by advection during hydration and desiccation. Generally, the extracellular pore-water equilibrate fastest to the surroundings, followed by the mycobiont, and lastly the photobiont lags closely behind the mycobiont. Hysteresis between hydration and desiccation periods is controlled by the nonlinearities in thallus water retention and hydraulic capacitance, supporting our second hypothesis. Linear or weakly nonlinear responses of thallus water retention and capacitance to water potential would prolong hydrated, active periods under drying conditions, enable quick hydration under wetting conditions, and thereby maximize the period of productivity. However, the nonlinearity of the water retention of *F. caperata* is considerable, which causes faster drying and slower wetting relative to the linear case. We believe this nonlinearity and resulting behavior may reflect *F. caperata*'s preference for humid and stable environments. Our model can reproduce observed dehydration and hydration dynamics of lichen and predict interactions between internal mycobiont, photobiont, and extracellular pore-space compartments. It can shed critical light on processes that are either impossible or difficult to directly study from laboratory experiments alone, such as the spatial and temporal distributions in water potential within the thallus that control internal water fluxes.

## ACKNOWLEDGMENTS

A.P. acknowledges the support of Rutgers University Academic Excellence Graduate Fellowship support. G.C.D. acknowledges support from the Department of Energy, Basic Energy Sciences, Grant DE-FG02-10ER16195. The authors are thankful to our anonymous reviewers who provided comments and recommendations to improve the scientific insights of the manuscript.

## AUTHOR CONTRIBUTIONS

A.P., G.C.D., G.A., and M.C.t.V. designed the laboratory experiments. A.P., G.A., and M.C.t.V. performed the measurements. A.P., Y.F., and C.R.C.M. designed the model. A.P. coded and ran the model and analyzed laboratory and simulated data. A.P., G.C.D., and M.C.t.V. led the writing. All authors contributed to data interpretation, discussion and the final version.

## SUPPORTING INFORMATION

Additional Supporting Information may be found in the online version of this article at the publisher's web-site.

## ORCID

Aaron Potkay  <https://orcid.org/0000-0003-3101-2701>

Marie-Claire ten Veldhuis  <https://orcid.org/0000-0001-9572-2193>

## REFERENCES

- Ahmadjian, V. V. (1993). *The Lichen Symbiosis*. NY: John Wiley & Sons.
- Ahmadjian, V. V. (1995). Lichens are more important than you think. *BioScience*, 45, 124.
- Blum, O. B. (1973). Water relations. In V. V. Ahmadjian & M. E. Hale (Eds.), *The Lichens* (pp. 381–400). NY: Academic Press.
- Coxson, D. (1991). Impedance measurement of thallus moisture content in lichens. *The Lichenologist*, 23, 77–84.
- Crittenden, P. D. (1991). Ecological significance of necromass production in mat-forming lichens. *Lichenologist*, 23, 323–331.
- Dahlman, L., & Palmqvist, K. (2003). Growth in two foliose tripartite lichens *Nephromaarcticum* and *Peligeriaaphthosa* – empirical modeling of external versus internal factors. *Functional Ecology*, 17, 821–831.
- De los Ríos, A., Ascaso, C., & Wierzechos, J. (1999). Study of lichens with different state of hydration by the combination of low temperature scanning electron and confocal laser scanning microscopies. *International Microbiology*, 2(4), 251–257.
- Emancipator, K., & Kroll, M. H. (1993). A quantitative measure of non-linearity. *Clinical Chemistry*, 39, 766–772.
- Eriksson, A., Gauslaab, Y., Palmqvista, K., Ekström, M., & Esseen, P. A. (2018). Morphology drives water storage traits in the globally widespread lichen genus *Usnea*. *Fungal Ecology*, 35, 51–61.
- Farquhar, G. D., von Caemmerer, S., & Berry, J. A. (1980). A biochemical model of photosynthetic CO<sub>2</sub> assimilation in leaves of C3 species. *Planta*, 149, 78–90.
- Franks, P. J., Cowan, I. R., & Farquhar, G. D. (1998). A study of stomatal mechanics using the cell pressure probe. *Plant, Cell & Environment*, 21, 94–100.
- Franks, P. J., Cowan, I. R., Tyerman, S. D., Cleary, A. L., Lloyd, J., & Farquhar, G. D. (1995). Guard-cell pressure aperture characteristics measured with the pressure probe. *Plant, Cell & Environment*, 18, 795–800.
- Gauslaa, Y., & Solhaug, K. A. (1998). The significance of thallus size for the water economy of the cyanobacterial old-forest lichen *Degelia plumbea*. *Oecologia*, 116, 76–84.
- Gerke, H. H., & van Genuchten, M. T. (1993). A dual-porosity model for simulating the preferential movement of water and solutes in structured porous media. *Water Resources Research*, 29, 305–319.
- Giordani, P., & Incerti, G. (2008). The influence of climate on the distribution of lichens: a case study in a borderline area (Liguria, NW Italy). *Plant Ecology*, 195, 257–272.
- Green, T. G. A., Sancho, L. G., & Pintado, A. (2011). Ecophysiology of desiccation/rehydration cycles in mosses and lichens. In U. Lüttge, E. Beck, & D. Bartels (Eds.), *Plant Desiccation Tolerance Ecological Studies* (Vol. 215, pp. 89–120). Berlin: Springer-Verlag.
- Heitman, J. L., Horton, R., Sauer, T. J., & DeSutter, T. M. (2008). Sensible heat observations reveal soil-water evaporation dynamics. *Journal of Hydrometeorology*, 9(1), 165–171.
- Helle, T., Aspi, J., & Tarvainen, L. (1983). The growth rate of *Cladonia rangiferina* and *C. mitis* in relation to forest characteristics in northeastern Finland. *Rangifer*, 3, 2–5.
- Hölttä, T., Lintunen, A., Chan, T., Mäkelä, A., & Nikinmaa, E. (2017). A steady-state stomatal model of balanced leaf gas exchange, hydraulics and maximal source–sink flux. *Tree Physiology*, 37(7), 851–868.
- Honegger, R. (1984). Cytological aspects of mycobiont-photobiont relationship in lichens. Haustorial types, phycobiont cell wall types, and the ultrastructure of the cell surface layers in some cultured and symbiotic myco- and phycobionts. *The Lichenologist*, 16, 111–127.
- Honegger, R. (1991). Functional aspects of lichen symbiosis. *Annual Reviews of Plant Physiology and Plant Molecular Biology*, 42, 553–578.
- Honegger, R. (1998). The lichen symbiosis – What is so spectacular about it? *The Lichenologist*, 30, 193–212.
- Honegger, R. (2006). Water relations in lichens. In G. M. Gadd, S. C. Watkinson, & P. Dyer (Eds.), *Fungi in the Environment* (pp. 185–200). Cambridge: Cambridge University Press.
- Honegger, R. (2012). The symbiotic phenotype of lichen-forming ascomycetes and their endo- and epibionts. In *Fungal Associations* (pp. 287–339). Berlin: Springer.

- Honegger, R., & Haisch, A. (2001). Immunocytochemical location of the (1 → 3) (1 → 4)-beta-glucan lichenin in the lichen-forming ascomycete *Cetrariaislandica* (Icelandic moss). *New Phytologist*, 150(3), 739–746.
- Honegger, R., & Peter, M. (1994). Routes of solute translocation and the location of water in heteromorous lichens visualized with cryotechniques in light and electron-microscopy. *Symbiosis*, 16(2), 167–186.
- Incerti, G., & Nimis, P. L. (2003). Biogeographical outline of epiphytic lichens in a Mediterranean area: Calabria (S-Italy). *The Lichenologist*, 38(4), 355–371.
- Jonsson, A. V., Moen, J., & Palmqvist, K. (2008). Predicting lichen hydration using biophysical models. *Oecologia*, 156(2), 259–273.
- Jonsson-Čabrajčić, A. V., Lidén, M., Lundmark, T., Ottosson-Löfvenius, M., & Palmqvist, K. (2010). Modelling hydration and photosystem II activation in relation to in situ rain and humidity patterns: a tool to compare performance of rare and generalist epiphytic lichens. *Plant, Cell & Environment*, 33, 840–850.
- Kershaw, K. A. (1985). *Physiological Ecology of Lichens*. Cambridge: Cambridge University Press.
- Kershaw, K. A., & Rouse, W. R. (1971). Studies on lichen-dominated systems. I. The water relations of *Cladoniaalpestris* in spruce-lichen woodland in northern Ontario. *Canadian Journal of Botany*, 49, 1389–1399.
- Kim, Y. X., & Steudle, E. (2007). Light and turgor affect the water permeability (aquaporins) of parenchyma cells in the midrib of leaves of *Zea mays*. *Journal of Experimental Botany*, 58(15–16), 4119–4129.
- Kosugi, M., Shizuma, R., Moriyama, Y., Koike, H., Fukunaga, Y., Takeuchi, A., ... Satoh, K. (2014). Ideal osmotic spaces for chlorobionts or cyanobionts are differentially realized by lichenized fungi. *Plant Physiology*, 166(1), 337–348.
- Kytöviita, M. M., & Crittenden, P. D. (2002). Seasonal variation in growth rate in *Stereocaulon paschale*. *Lichenologist*, 34, 533–537.
- Lai, S., Tiedje, J. M., & Erickson, A. E. (1976). In situ measurement of gas diffusion coefficient in soils. *Soil Science Society of America Journal*, 40, 3–6.
- Lang, A. (1978). A model of mass flow in the phloem. *Australian Journal of Plant Physiology*, 5, 535–546.
- Lange, O. L., Büdel, B., Heber, U., Meyer, A., Zellner, H., & Green, T. G. A. (1993). Temperate rainforest lichens in New Zealand: high thallus water content can severely limit photosynthetic CO<sub>2</sub> exchange. *Oecologia*, 95, 303–313.
- Lange, O. L., Geiger, I. L., & Schulze, E. D. (1977). Ecophysiological investigations on lichens of the Negev Desert. V. A model to simulate net photosynthesis and respiration of *Ramalinamaciformis*. *Oecologia*, 34, 89–100.
- Lange, O. L., Green, T. G. A., & Heber, U. (2001). Hydration-dependent photosynthetic production of lichens: What do laboratory studies tell us about field performance? *Journal of Experimental Botany*, 52, 2033–2042.
- Lesmerises, R., Ouellet, J. P., & St-Laurent, M. H. (2011). Assessing terrestrial lichen biomass using ecoforest maps: A suitable approach to plan conservation areas for forest-dwelling caribou. *Canadian Journal of Forest Research*, 41(3), 632–642.
- Lidén, M., Jonsson-Čabrajčić, A. V., Ottosson-Löfvenius, M., Palmqvist, K., & Lundmark, T. (2010). Species-specific activation time lags can explain habitat restrictions in hydrophilic lichens. *Plant Cell & Environment*, 33(5), 851–862.
- Lloyd, C. R. (2001). The measurement and modelling of the carbon dioxide exchange at a high Arctic site in Svalbard. *Glob Change Biology*, 7, 405–426.
- Longton, R. E. (1988). *Biology of Polar Bryophytes and Lichen* (Vol. 1). Cambridge: Cambridge University Press.
- McCulloh, K. A., Johnson, D. M., Meinzer, F. C., & Woodruff, D. R. (2014). The dynamic pipeline: hydraulic capacitance and xylem hydraulic safety in four tall conifer species. *Plant, Cell & Environment*, 37, 1171–1183.
- Meidner, H., & Edwards, M. (1975). Direct measurements of turgor pressure potentials of guard cells. *Journal of Experimental Botany*, 26, 319–330.
- Meinzer, F. C., Johnson, D. M., Lachenbruch, B., McCulloh, K. A., & Woodruff, D. R. (2009). Xylem hydraulic safety margins in woody plants: coordination of stomatal control of xylem tension with hydraulic capacitance. *Functional Ecology*, 23, 922–930.
- Monteith, J. L. (1965). Evaporation and the environment. *Symposium of the Society of Experimental Biology*, 19, 205–234.
- Palmqvist, K., & Sundberg, B. (2000). Light use efficiency of dry matter gain in five macro-lichens: relative impact of microclimate and species-specific traits. *Plant, Cell & Environment*, 23, 1–14.
- Paterson, D. R., Paterson, E. W., & Kenworthy, J. B. (1983). Physiological studies on temperate lichen species I. A mathematical model to predict assimilation in the field, based on laboratory responses. *The New Phytologist*, 94, 605–618.
- Péché, G. Y. (1989). A model to predict the moisture content of reindeer lichen. *Forest Science*, 35, 1014–1028.
- Penman, H. L. (1948). Natural evaporation from open water, bare soil and grass. *Proceedings of the Royal Society of London, Series A, Mathematical and Physical Sciences*, 193, 120–145.
- Philip, J. R. (1969). Hydrostatics and hydrodynamics in swelling soils. *Water Resources Research*, 5, 1070–1077.
- Philip, J. R., & de Vries, D. A. (1957). Moisture movement in porous materials under temperature gradients. *Transactions American Geophysical Union*, 38(2), 222–232.
- Potkay, A. (2017). One-dimensional seepage in unsaturated, expansive soils. *Vadose Zone Journal*, 169(11), 1–6.
- Richards, L. A. (1931). Capillary conduction of liquids through porous medium. *Physics*, 1, 318–333.
- Richardson, L. F. (1922). *Weather Prediction by Numerical Process* (p. 262). Cambridge: University Press.
- Rundel, P. W. (1998). Water relations. In M. Galun (Ed.), *CRC Handbook of Lichenology* (Vol. 2, pp. 17–36). Boca Raton: CRC Press.
- Rundel, P. W. (1982). The role of morphology in the water relations of desert lichens. *The Journal of the Hattori Botanical Laboratory*, 53, 315–320.
- Sanders, W. B., & Ríos, A. (2017). Parenchymatous cell division characterizes the fungal cortex of some common foliose lichens. *American Journal of Botany*, 104, 207–217.
- Selosse, M. A. (2002). Prototaxites: a 400 Myr old giant fossil, a saprophytic basidiomycete or a lichen? *Mycological Research*, 106, 642–644.
- Selosse, M. A., Strullu-Derrien, C., Martin, F. M., Kamoun, S., & Kenrick, P. (2015). Plants, fungi and oomycetes: a 400-million year affair that shapes the biosphere. *New Phytologist*, 206, 501–506.
- Smiles, D. E., & Rosenthal, M. J. (1968). The movement of water in swelling materials. *Australian Journal of Soil Research*, 6, 237–248.
- Sundberg, B., Näsholm, T., & Palmqvist, K. (2001). The effect of nitrogen on growth and key thallus components in the two tripartite lichens, *Nephromaarcticum* and *Peltigeraaphthosa*. *Plant, Cell & Environment*, 24, 517–527.
- Sveinbjörnsson, B. (1987). Reindeer lichen productivity as a function of mat thickness. *Arctic Alpine Research*, 19, 437–441.
- Ten Veldhuis M.C., Dismukes G.C. & Ananyev G. (2017) Hydrology in lichens: how biological architecture is used to regulate water access to support drought resilience and nutrient transport. In *AGU Fall Meeting Abstracts*.
- Tenhunen, J. D., Yocum, C. S., & Gates, D. M. (1976). Development of a photosynthesis model with an emphasis on ecological adaptations I. *Theory Oecologia*, 26, 89–100.
- Tetens, O. (1930). Über einige meteorologische Begriffe. *Zeitschrift für Geophysik*, 6, 207–309.
- Thompson, M. V., & Holbrook, N. M. (2003). Application of a single solute non-steady-state phloem model to the study of long-distance assimilate transport. *Journal of Theoretical Biology*, 220, 419–455.

- Tyree, M. T. (1970). The symplast concept: a general theory of symplastic transport according to the thermodynamics of irreversible processes. *Journal of Theoretical Biology*, 26, 181–214.
- van Genuchten, M. T. (1980). A closed-form equation for predicting the hydraulic conductivity of unsaturated soils. *Soil Science Society of American Journal*, 44, 892–898.
- Vico, G., & Porporato, A. (2008). Modelling C-3 and C-4 photosynthesis underwater-stressed conditions. *Plant and Soil*, 313, 187–203.
- Voortman, B. R., Bartholomeus, R. P., van Bodegom, P. M., Gooren, H., van der Zee, S. E., & Witte, J. P. M. (2014). Unsaturated hydraulic properties of xerophilous mosses: Towards implementation of moss covered soils in hydrological models. *Hydrological Processes*, 28, 6251–6264.
- Zimmermann, U., & Steudle, E. (1975). The hydraulic conductivity and volumetric elastic modulus of cells and isolated cell walls of *Nitella* and *Chara* spp.: Pressure and volume effects. *Functional Plant Biology*, 2, 1–12.

## SUPPORTING INFORMATION

Additional supporting information may be found online in the Supporting Information section at the end of this article.

**How to cite this article:** Potkay A, ten Veldhuis M-C, Fan Y, Mattos CRC, Ananyev G, Dismukes GC. Water and vapor transport in algal-fungal lichen: Modeling constrained by laboratory experiments, an application for *Flavoparmelia caperata*. *Plant Cell Environ*. 2020;43:945–964. <https://doi.org/10.1111/pce.13690>